OULU 2011
D 1128

ACTA UNIVERSITATIS OULUENSIS

Jérôme Thevenot

BIOMECHANICAL ASSESSMENT OF HIP FRACTURE

DEVELOPMENT OF FINITE ELEMENT MODELS TO PREDICT FRACTURES

UNIVERSITY OF OULU,
FACULTY OF MEDICINE,
INSTITUTE OF BIOMEDICINE,
DEPARTMENT OF MEDICAL TECHNOLOGY

ACTA UNIVERSITATIS OULUENSIS
D Medica 1128

JÉRÔME THEVENOT

BIOMECHANICAL ASSESSMENT OF HIP FRACTURE

Development of finite element models to predict fractures

Academic dissertation to be presented with the assent of the Faculty of Medicine of the University of Oulu for public defence in Auditorium A101 of the Department of Anatomy and Cell Biology (Aapistie 7 A), on 25 November 2011, at 12 noon

UNIVERSITY OF OULU, OULU 2011

Acta Univ. Oul. D 1128, 2011

Supervised by
Professor Timo Jämsä

Reviewed by
Professor Christian Langton
Docent Rami Korhonen

ISBN 978-951-42-9609-3 (Paperback)
ISBN 978-951-42-9610-9 (PDF)

ISSN 0355-3221 (Printed)
ISSN 1796-2234 (Online)

Cover Design
Raimo Ahonen

JUVENES PRINT
TAMPERE 2011

Thevenot, Jérôme, Biomechanical assessment of hip fracture. Development of finite element models to predict fractures

University of Oulu, Faculty of Medicine, Institute of Biomedicine, Department of Medical Technology, P.O. Box 5000, FI-90014 University of Oulu, Finland

Acta Univ. Oul. D 1128, 2011
Oulu, Finland

Abstract

Hip fracture is the most severe complication of osteoporosis. The occurrence of hip fracture is increasing worldwide as a result of the ageing of the population. The clinical assessment of osteoporosis and to some extent hip fracture risk is based on the measurement of bone mineral density (BMD) using dual X-ray absorptiometry (DXA). However, it has been demonstrated that most hip fractures occurring after a fall involve non-osteoporotic populations and that the geometry plays a critical role in the fracture risk assessment. A potential alternative for the assessment of hip fracture risk is finite element modelling, which is a computational method allowing simulation of mechanical loading. The aim of this study was to investigate different finite-element (FE) methods for predicting hip fracture type and eventually hip failure load in the simulation of a fall on the greater trochanter.

An experimental fall on the greater trochanter was performed on over 100 cadaver femurs in order to evaluate the failure load and fracture type. In all studies, assessment of BMD, measurement of geometrical parameters and generation of finite element models were performed using DXA, digitized plain radiographs and computed tomography scans.

The present study showed that geometrical parameters differ between specific hip fracture types. FE studies showed feasible accuracy in the prediction of hip fracture type, even by using homogeneous material properties. Finally, a new method to generate patient-specific volumetric finite element models automatically from a standard radiographic picture was developed. Preliminary results in the prediction of failure load and fracture type were promising when compared to experimental fractures.

Keywords: biomechanics, cervical fracture, computed tomography, failure load, finite element, fracture risk, hip fracture, patient-specific models, radiography, trochanteric fracture

Thevenot, Jérôme, Lonkkamurtuman biomekaaninen arviointi. Elementtimallien kehittäminen murtumien ennustamiseen
Oulun yliopisto, Lääketieteellinen tiedekunta, Biolääketieteen laitos, Lääketieteen tekniikka, PL 5000, 90014 Oulun yliopisto
Acta Univ. Oul. D 1128, 2011
Oulu

Tiivistelmä

Lonkkamurtuma on osteoporoosin vakavin seuraus. Lonkkamurtumatapaukset kasvavat maailmanlaajuisesti väestön ikääntymisen myötä. Osteoporoosin ja osin myös lonkkamurtumariskin kliininen arviointi perustuu luun mineraalitiheyden mittaamiseen kaksienergisellä röntgenabsorptiometrialla (Dual-energy X-ray absorptiometry, DXA). On kuitenkin osoitettu, että suurin osa kaatumisen seurauksena tapahtuvista lonkkamurtumatapauksista tapahtuu henkilöillä joilla ei ole todettua osteoporoosia, ja että myös luun muoto on tärkeä tekijä arvioitaessa lonkkamurtumariskiä. Laskennallinen mallintaminen elementtimenetelmällä mahdollistaa mekaanisen kuormituksen simuloinnin ja on potentiaalinen vaihtoehto lonkkamurtumariskin arviointiin. Tämän työn tarkoituksena on tutkia elementtimenetelmiä lonkkamurtumatyypin ja lopulta lonkan murtolujuuden ennustamiseksi simuloimalla kaatumista sivulle.

Yli sataa reisiluuta kuormitettiin kokeellisesti murtolujuuden ja murtumatyypin määrittämiseksi. Luun mineraalitiheyden arviointi, muotoparametrien mittaus ja elementtimallit tehtiin käyttäen DXA:a, digitalisoituja röntgenkuvia ja tietokonetomografiakuvia.

Tämä tutkimus osoittaa, että luun muotoparametrit vaihtelevat eri lonkkamurtumatyyppien välillä. Lonkkamurtumatyyppi voitiin ennustaa hyvällä tarkkuudella elementtimenetelmän avulla silloinkin, kun käytettiin homogeenisia materiaaliominaisuuksia. Lopuksi kehitettiin uusi menetelmä yksilöllisten kolmiulotteisten elementtimallien automaattiseen luontiin tavallisista röntgenkuvista. Alustavat tulokset lonkan murtolujuuden ja murtumatyypin ennustamisessa ovat lupaavia.

Asiasanat: biomekaniikka, elementtimenetelmä, kaulamurtuma, lonkkamurtuma, murtolujuus, murtumariski, röntgenkuvaus, sarvennoismurtuma, tietokonetomografia, yksilölliset mallit

To my family

Acknowledgments

This study was carried out at the Institute of Biomedicine, Department of Medical Technology at the University of Oulu, during the years 2006–2011. Thanks to the excellent conditions offered by the department, it has been pleasure for me to work here during all these years.

I would like to express my deep and sincere gratitude to my supervisor, Professor Timo Jämsä; his encouraging and personal guidance have helped me in many ways during the project. I am glad that he offered me the chance to work under his supervision, and that he always found time for discussions with me, despite my field being somewhat different from that of the department. I wish to thank my other Finnish co-authors, MSc Janne Koivumäki and PhD Pasi Pulkkinen, for their fruitful contribution to the thesis. In particular, I would like to thank Janne Koivumäki for the time we spent together developing our models and his large contribution in the post-processing part of the last study. Pasi Pulkkinen is especially acknowledged for statistical advice. I wish to thank my international co-authors, Prof. Felix Eckstein and Dr Volker Kuhn, for the experimental part of the study and the expert criticism they provided during the study.

I am very grateful to the official referees of this thesis, Docent Rami Korhonen from the University of Kuopio and Prof. Chris Langton from Queensland University of Technology, for their careful revision of the manuscript and their valuable comments.

I also want to thank MD, Prof. Miika Nieminen for answering all my questions from a clinical point of view and for the help he provided in scheduling access to the segmentation machine in the Department of Radiology for me and Janne. I also wish to thank Anna Vuolteenaho for revision of the language of this thesis.

I would like to warmly thank the staff of the Department of Medical Technology; you answered my endless questions and helped me with the difficulties and incomprehension I faced in daily life. Riikka, Mikko and Maarit, I thank you for the everyday support and all the discussions we had together. I really enjoyed the time I spent with you, as co-workers of course, but also as friends. Mikko Finnilä, I thank you for the talks we had about our professional life, but also about our shared interest in gastronomy and sports, you really have some social skills… I also would like to thank all the students who have been working with me on programming and image processing.

I will not forget to thank my friends; they showed me what Finnish culture is. They were with me when I was boiling in sauna, freezing in an iced-up river, eaten alive by mosquito while fishing… but all in all, they were there for me when I needed them and for sure, if I like Finland so much, they are one of the reasons why. I would like to thank Heikki Rantala, Pekka Mankila, Tytti Luikku, Thystere Bangue-Tandet, Minna Pulla-Rantala, Eija Junttila, Annika Juvani, Sandra Juutilainen, Jukka Junell, Teemu Kyllönen, Virpi Evesti and the ESN people… and all my friends outside the academia.

Finally, I want to thank my family for their support. Mum and dad, thank you for helping me despite the distance. Audrey and Cindy, thanks to you for supporting your brother. I want also to thank my cousin Franck and his wife Stephanie: you always welcomed me and my friends in your house with open arms, we always have enjoyable moments together, and I hope it will continue.

This study was financially supported by the International Graduate School in Biomedical Engineering and Medical Physics, the National Doctoral Programme of Musculoskeletal Disorders and Biomaterials, the Finnish Funding Agency for Technology and Innovation, and the Association Franco-Finlandaise pour la Recherche Scientifique et Technique.

Abbreviations

Δ	Difference of two values
α	Angle
ε	Strain
σ	Stress
ρ_{app}	Apparent density
ρ_{ash}	Ash density
μ	Shear modulus
ν	Poisson's ratio
A	Area
ANCOVA	Analysis of covariance
AO	Arbeitsgemeinschaft für Osteosynthesefragen
ASM	Active shape modelling
BMD	Bone mineral density
C	Cervical fracture
CFC	Medial calcal femoral cortical thickness
CSA	Cross-sectional area
CSMI	Cross-sectional moment of inertia
CT	Computed tomography
DXA	Dual-energy X-ray absorptiometry
E	Young's modulus
EPOS	European Prospective Osteoporosis Study
F	Force
FEBMD	femoral neck bone mineral density
FE	Finite element
FEM	Finite element modelling
FNAL	Femoral neck axis length
FRAX®	WHO Fracture Risk Assessment Tool
FSC	Femoral shaft cortical thickness
FSD	Femoral shaft diameter
GLCM	Gray-level co-occurrence matrix
HAL	Hip axis length
HD	Femoral head diameter
HI	Homogeneity index
HSA	Hip structural analysis
HU	Hounsfield unit

l	Length
MRI	Magnetic resonance imaging
ND	Femoral neck diameter
NIH	National Institute of Health
NSA	Femoral neck-shaft angle
PCS	Principal trabecular compressive system
PTS	Principal trabecular tensile system
QCT	Quantitative computed tomography
ROC	Receiver operating characteristic curve
ROI	Region of interest
RMS CV	Root-mean-square average of coefficient of variation
S	Shaft fracture
SD	Standard deviation
SSM	Statistical shape modelling
STL	Stereolitographic format
T	Trochanteric fracture
TMO	Trabecular main orientation
TRBMD	Trochanteric bone mineral density
TW	Trochanteric width
UFNBMD	Upper femoral neck bone mineral density
vBMD	Volumetric bone mineral density
VXA	Volumetric DXA
WABMD	Ward’s triangle bone mineral density
WHO	World Health Organization

List of original publications

The thesis consists of four original articles that are referred to in the text by their Roman numerals (I-IV).

I Thevenot J, Pulkkinen P, Kuhn V, Eckstein F & Jämsä T (2010) Structural asymmetry between the hips and its relation to experimental fracture type. Calcified Tissue International 87(3): 203–210.

II Thevenot J, Pulkkinen P, Koivumäki J, Kuhn V, Eckstein F & Jämsä T (2009) Discrimination of Cervical and Trochanteric Hip Fractures Using Radiography-Based Two-Dimensional Finite Element Models. Open Bone Journal 1: 16–22.

III Koivumäki J, Thevenot J, Pulkkinen P, Salmi J, Kuhn V, Lochmüller E-M, Link T, Eckstein F & Jämsä T (2010) Does femoral strain distribution coincide with the occurrence of cervical vs. trochanteric hip fractures? Medical & Biological Engineering & Computing 48(7): 711–717.

IV Thevenot J, Koivumäki J, Pulkkinen P, Kuhn V, Eckstein F & Jämsä T (2011) Estimation of experimental hip fracture load using 3D finite element models derived from plain radiographs. Manuscript.

Contents

1 Introduction

Hip fracture is considered the most serious complication of osteoporosis, and due to ageing of the population, its occurrence is increasing worldwide. Clinically, the diagnosis of osteoporosis is based on the amount of mineral per area, measured using dual-energy x-ray absorptiometry (DXA). However, it has been demonstrated that the bone mineral density (BMD) assessed from DXA-based images is insufficient to accurately predict individual hip fracture risk (Burr 2002, Kanis 2002, Schuit *et al.* 2004), the majority of hip fractures occurring in people not considered osteoporotic (Cummings 1985, Stone *et al.* 2003, Schuit *et al.* 2004).

Falls have been shown to be the primary reason for the occurrence of hip fracture (Grisso *et al.* 1991a), 90% of them estimated to be originated by a fall (Youm *et al.* 1999a). Bone is able to adapt to its usual loading environment (Wolff 1892, Frost 1994, 2004). However, a fall will involve unusual load intensity and direction (Currey 2003a, 2003b, Sievänen & Kannus 2007a) that might exceed the bone strength (Currey 2001),

Different classifications have been presented to classify fracture types (Evans 1949, Ramadier *et al.* 1956, Garden 1961, Briot 1980 Müller 1980, Müller & Nazarian 1981). In the AO classification, related to options of actual surgical procedures for fixation, three main groups are defined: trochanteric, cervical and femoral head fractures. However, it has been shown that fracture types have different risk factors (Duboeuf *et al.* 1997, Partanen *et al.* 2001, Gnudi *et al.* 2002, Szulc *et al.* 2006) and should be evaluated separately (Mautalen *et al.* 1996). Studies on fracture types also revealed that while cervical fractures are related to low impact (Pulkkinen *et al.* 2006), trochanteric fractures involve higher mortality (Haentjens *et al.* 2007). Finally, the occurrence of a specific fracture type is highly dependent on gender (Baudoin *et al.* 1993).

Finite element modelling (FEM) is a computational method allowing estimation of stress and strain distribution during simulation of various mechanical loading situations. When applied to biological tissues, generation of patient-specific models is available using different medical imaging modalities with relevant results in bone strength assessment (Cody *et al.* 1999, Crawford *et al.* 2003). It has been shown that both geometry and structure of the hip are essential in the identification of patients at high risk (Cody *et al.* 2000a, 2000b, Lochmüller *et al.* 2002, Bergot *et al.* 2002, Duan *et al.* 2003, Gregory *et al.* 2004a, 2004b, 2005, 2007, 2008). Despite being accurate when compared with

experimental simulations (Keyak *et al.* 2001, Keyak & Falkinstein 2003, Bessho *et al.* 2007, Schileo *et al.* 2007, 2008), computed tomography (CT) based models are time-consuming and costly. Alternative methods to generate volumetric models have been developed lately (Sadowsky *et al.* 2007, Gregory *et al.* 2007, Langton *et al.* 2009a, 2009b, Zheng *et al.* 2009, Zheng & Schumann 2009, Bryan *et al.* 2009, 2010, Schumann *et al.* 2010), but further studies need to be accomplished before they are clinically applicable.

This study focused on the prediction of the fracture type and failure load using FEM from different medical imaging modalities by mimicking an experimental simulation of a fall on the greater trochanter (Eckstein *et al.* 2004). The impact of the upper femur geometry in the variation of fracture type and failure load was evaluated to characterize the mechanical behaviour of the bone under controlled conditions. The final purpose of the study was to obtain an accurate computational model to assess fracture type and failure load based on data extracted from a standard radiograph.

2 Review of the literature

2.1 Overview of the structure and physiology of bone

Bones are tissues with high density; their organization in the whole body composes the skeleton, the structure that allows the rigidity of the human body. The main function of bone is its capability of not deforming too much under a certain amount of loading (Currey 2003b). In addition, bones are important for mineral metabolism.

The shapes and structures of bones vary depending on their function. The hip area, and especially the femur, support the upper part of the body and allow locomotion of an individual by its interaction with the muscles. The following chapter will focus on the anatomy of the femur.

2.1.1 Structure

As a composite material, bone is made up of inorganic mineral content (up to 70%) and water as well as extracellular matrix. Bones are surrounded on their surface by the periosteum, which is a thin membrane that allows insertion of both ligaments and tendons. The role of the periosteum is to assure blood supply to both bones and skeletal muscles. It has also been shown to have a major role in bone growth and bone repair (Seeman 2007, Dweck 2010). The areas of bone that are not covered by periosteum are instead covered by another connective tissue, cartilage.

Bone includes two compartments: the trabecular bone and the cortical bone surrounding it. Each of these structures has different architecture and density, the cortical bone being more compact than the trabecular bone and representing the bending resistance of the bone (Seeman & Delmas 2006, Seeman 2008). However, it has been demonstrated that the trabecular bone is metabolically more active, and more affected by remodelling (Wolff 1892, Roesler 1987), its architecture being highly correlated with strength.

Geometry of the femur

The femur is the longest bone in the human body, providing connections between the body at the pelvis and the lower limbs at the knee. The upper femur has a

complex geometry that can be divided into subparts (Fig. 1) with different functions. The femoral head, with its half-spherical shape and its smooth surface covered by cartilage, constitutes a direct connection with the pelvis through the *acetabulum*, forming the hip joint. The lower part of the centre of the head reveals the presence of ligaments connected to the acetabulum and providing stabilizing strength. The femoral neck is the support of the femoral head, connecting it to the femoral shaft with a diameter of almost half of the femoral head diameter. The axis of the femoral neck towards the axis of the femoral shaft is defined by an angle called neck-shaft angle (NSA). The trochanteric area has a complex geometry due to the presence of muscle, ligament and tendon connections. The cortical bone is the thickest in the shaft, and its thickness decreases progressively in the neck area to finally becoming a thin layer, comparable to a shell covering the trabecular bone of the upper areas of the trochanter and femoral head. Finally, the shaft constitutes the body of the femur and connects the upper femur with the lower femur. (Fig. 1).

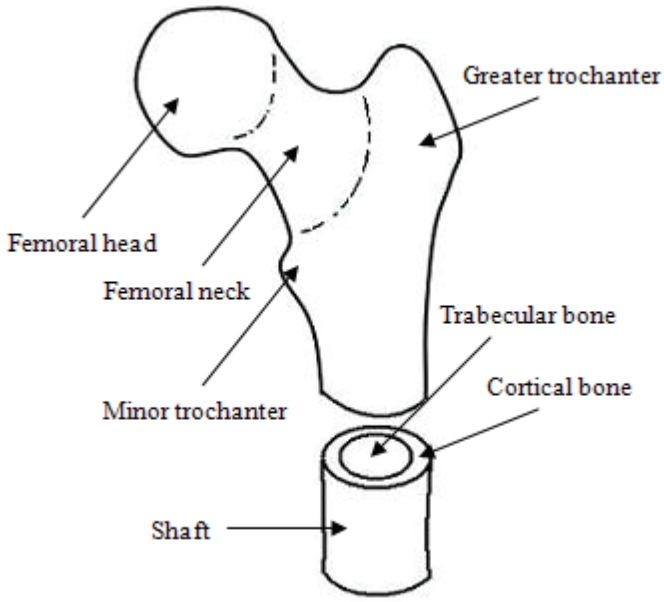

Fig.1. Parts of the upper femur.

Dimensions of the bones are highly dependent on the size of the whole body. The existence of asymmetries in both the upper and lower limbs between left and right sides has been demonstrated (Auerbach & Ruff 2006). The left side often being the supportive limb, as explained by the cross-symmetrical side dominance with the upper limbs (Auerbach & Ruff 2006, Kanchan *et al.* 2008), it has been hypothesized that lower limbs have a structural and functional asymmetry (Cuck *et al.* 2001, Samaha *et al.* 2008). While focusing on the upper femur area, it has been shown that hip dimensions are higher on the left side than on the right side (Macho 1991, Cuck *et al.* 2001, Brownbill *et al.* 2003), except for the femoral shaft diameter (Macho 1991).

2.1.2 Bone adaptation

The growing and ageing skeleton

During the lifespan, the skeleton adapts itself to ageing, daily activity and all environmental factors with direct impact on the body. For example, in order to maintain its functions, such as locomotion and supportive function, the femur has to adapt its shape, structure and position to changes in daily loading orientations and levels (Seeman & Delmas 2006).

Bone mass increases from childhood until the end of adolescence, when it achieves its peak (Haapasalo *et al.* 1996) as a result of natural changes in bone length and size. As adult age is reached, bone mass will start to decrease gradually, with a difference between men and women. As a result of hormonal changes, bone mass will decrease much faster in women (Riggs *et al.* 2004), especially after menopause.

It has been demonstrated that later in life, to compensate for bone loss, the femoral neck diameter tends to expand slowly (Heaney *et al.* 1997, Crabtree *et al.* 2000, Beck *et al.* 2000, 2001, Kaptoge *et al.* 2003, Meta *et al.* 2006, Gregory *et al.* 2007) as well as the bone size in the trochanter (Meta *et al.* 2006). It also has been reported that NSA tends to decrease with ageing (Isaac *et al.* 1997). However, due to greater loss of trabecular and cortical bone in the femoral neck than in the trochanter, this enlargement is insufficient to protect against loss of bone strength (Riggs *et al.* 2004, Mayhew *et al.* 2005, Meta *et al.* 2006).

Bone adaptation to loading

The internal structure of the bone is adapted to environmental conditions and to the daily loadings. These modifications allow the bone to maintain its strength to adapt it to the external mechanical environment. As suggested already at the end of the 19th century (Wolff 1892) by Wolff's law, the trabecular bone architecture is determined by the habitual stresses applied to the bones. Studies have been conducted to evaluate the impact of exercise on the BMD per region in the hip in order to focus on the benefits for bone (Wolff *et al.* 1999, Wallace & Cumming 2000). The characteristics of impact exercises have been shown to play a key role in bone maintenance or regeneration (Turner 1998, Gregg *et al.* 2000, Hans *et al.* 2002, Burr *et al.* 2002, Robling *et al.* 2002, Turner & Robling 2003, Robling *et al.* 2006, Jämsä *et al.* 2006, Barry & Kohrt 2008, Kam *et al.* 2009).

Modelling and remodelling

In order to constantly renew itself, the bone undergoes strictly regulated processes known as modelling and remodelling. While modelling consists of changes in both size and shape of the bone, remodelling is the maintenance that keeps up bone strength during adulthood. Osteoblasts are cells that allow the synthesis and mineralization of bone whereas osteoclasts are responsible for its resorption (Eriksen 2010). During the remodelling, both of these cell types act in teams called Bone Multicellular Units, first with resorption of the bone surface by osteoclasts followed by bone formation by osteoblasts (Eriksen 2010). It has been reviewed that osteocytes (osteoblasts trapped in the matrix they secreted) act as an orchestrator of bone remodelling through the regulation of cell activity (Bonewald 2011). Bone remodelling is essential for dealing with micro-damage, repairing dead bone or adapting to changes in local mechanical loadings.

The balance between resorption and formation of bone is the key of bone maintenance; however, some pathological conditions can affect this complex mechanism (Neve *et al.* 2011). In pathological bones suffering from osteoporosis, the proliferation of osteoblasts is reduced and their function showed to be defective compared to non-pathological bone (Neve *et al.* 2011). This lack of effectiveness in bone formation involves bone loss (Seeman & Delmas 2006).

2.1.3 Osteoporosis and osteopenia

Osteoporosis is a complex disorder of bone tissue which increases with the age of an individual. Due to hormonal changes occurring during menopause, older women are more affected by this disease than men. Osteoporosis is directly related to the decrease of bone mineral density affecting the microstructure of the bone, and explains the lowering of bone strength, and ultimately, the predisposition for higher risk of fracture (as stated by the NIH, Consensus Development Conference Statement 2000).

Clinically, the diagnosis of osteoporosis is based on the amount of mineral per area of interest in the hip, measured using dual-energy x-ray absorptiometry (DXA). A classification system for osteoporosis for women based on BMD was established in 1994, as a result of a working group of the World Health Organization (WHO 1994, Kanis 1994). By establishing a relationship between the BMD and the lifetime risk of fracture in the population, the working group was able to describe categories corresponding to the level of osteoporosis. As a result, the BMD of a subject can be compared to the mean BMD value at the femoral neck of a young healthy population, the reference being women 20–29 years of age (Kanis *et al.* 2008a). The difference is expressed in standard deviation (SD) units also referred to as T-score; 0 indicates BMD equal to the young adult mean; deviation above the mean is defined with positives values and below in negatives values (Table 1). The T-score is calculated using the following formula (U.S. Department of Health and Human Services 2004):

$$\text{T-Score} = \frac{\left(\text{Patients BMD -Young normal mean BMD}\right)}{\text{Standard Deviation of young normal mean}} \quad (1)$$

Table 1. Diagnostic categories for osteoporosis determined with DXA. Adapted from Kanis *et al.* (2005).

T-score value	Diagnostic categories
T-score > −1	Normal BMD
−2.5 < T-score ≤ −1	Osteopenia
T-score ≤ −2.5	Osteoporosis
T-score ≤ −2.5 + presence of one or more fragility fractures	Severe osteoporosis

Recently, WHO has developed the FRAX® tool to evaluate patients' fracture risk (Kanis *et al.* 2008b). It is based on integrating the risks associated with clinical

risk factors as well as bone mineral density at the femoral neck and gives a 10-year risk of fracture.

2.2 Upper femur fractures

Hip fractures have long been recognized as a major public health problem as a result of the ageing of the population. The incidence of hip fracture increases dramatically with age, so that about 90 percent of hip fractures occur after age 70 years (Melton 1996, Cummings & Melton 2002). White women have a twofold risk compared to white men (Gullberg *et al.* 1997, Cheng *et al.* 2009), while black women and men are at similar risk (Farmer *et al.* 1984). Although most falls are not associated with fractures in the elderly, over 90 percent of hip fractures are results of a fall (Grisso *et al.* 1991a, 1991b, Youm *et al.* 1999a, Parkkari *et al.* 1999).

2.2.1 Epidemiology of osteoporotic fractures

Osteoporotic fracture has been defined as a fracture occurring at a site associated with low BMD. Fractures occurring in other locations than the hip can be considered osteoporotic fractures as well. The sites concerned are the vertebras, wrist-forearm, humerus, other femoral areas, ribs, pelvis, clavicles, scapula and sternum, tibias and fibulas (Kanis *et al.* 2001).

Among all of these fractures, hip fractures are the most severe and they typically result in hospitalization for surgery. Even if treated, mortality occurs from 20% to 30% during the first year after fracture, this percentage being even higher for population with reduced mental or somatic health and low physical ability (Keene *et al.* 1993, Meyer *et al.* 2000, Johnell *et al.* 2004, Alegre-Lopez *et al.* 2005, Bentler *et al.* 2009, Da Costa *et al.* 2009, Ozturk *et al.* 2010).

Only half of hip fracture patients regain their ability to walk and independence at home; this is mostly due to an increase in long-term disability resulting in the need for aid at home (Sernbo & Johnell 1993, Hochberg *et al.* 1998, Youm *et al.* 1999b, Willig *et al.* 2001, Marks *et al.* 2003, Morita *et al.* 2005).

Hip fracture risk increases with age (Kanis 2002), due to a decrease in BMD and an increase in falls. In Scandinavia, the mean age of hip fracture has been reported to be 80 years (Kanis 2002). In Finland, the occurrence of hip fracture is constantly increasing, which is partially explained by demographic changes

(Boyce & Vessey 1985, Kannus *et al.* 1996, 1999, Luthje *et al.* 2009). However, a study by Kannus *et al.* (2006) demonstrated that the rise in hip fractures in the 1970s and 1990s has stopped and is now followed by a decline in fracture rates. There are lot of disparities between different countries, and Northern Europe has higher rates than Southern Europe (Kanis 2002).

2.2.2 Hip fracture types

Hip fractures are subdivided into categories regarding the location of the crack, the displacement of the femoral head and the severity of the fracture. Different classifications for the type of the fracture have been described (reviewed by Mabesoone 1997), such as Evans' classification (1949), Ramadier's classification (1956), Garden's classification (1961), Briot's classification (1980) and finally the AO classification proposed by Müller & Nazarian (1980, 1981) that will be described here.

In the AO classification, fracture types are divided into three main groups: trochanteric, cervical, and femoral head fractures. The sub-types of trochanteric and cervical fractures are presented in Fig. 2 and Fig. 3. Fractures of the femoral head are rare, being the result of an injury of the hip joint.

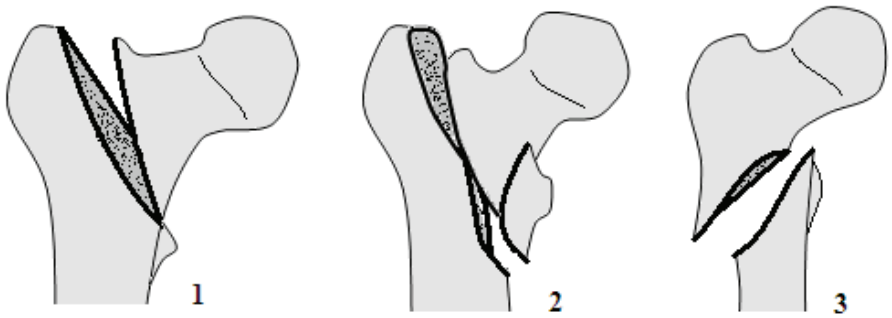

Fig. 2. Trochanteric fractures. (1) Simple fracture being cervicotrochanteric, pertrochanteric or trochanterodiaphyseal, (2) multiple fractures in the pertrochanteric area and (3) intertrochanteric fractures.

As an indication of estimating the severity of a cervical fracture, the displacement of the femoral neck has to be taken into account. It has been shown that cervical fractures with displacement of the femoral neck are more severe than cervical

fractures without displacement; displacement might affect the blood supply of the femoral head and eventually lead to necrosis (Fox *et al.* 2000). Supporting this statement, Cornwall *et al.* (2004) reported higher mortality rates among patients with displaced femoral neck. A recent study from Cauley *et al.* (2009) evaluated the different risk factors for severe hip fractures and concluded that a patient with high BMD will more likely have higher displacement of the femoral neck.

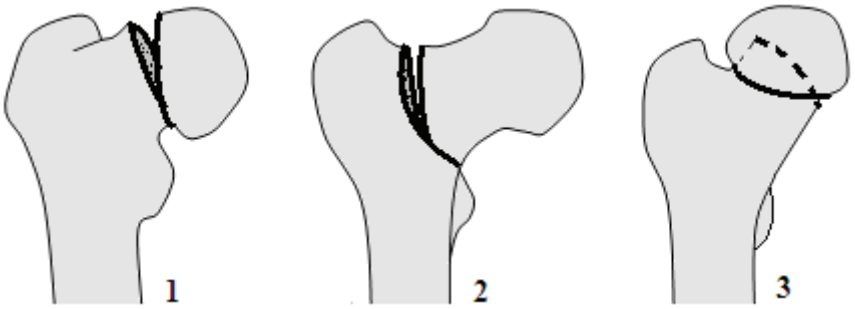

Fig. 3. Cervical fractures. (1) Subcapital fracture without displacement or valgus displacement, (2) transcervical fracture and (3) subcapital fracture with varus displacement or considerable displacement.

2.2.3 Risk factors for a hip fracture

The clinical risk factors

Many studies have been conducted to evaluate primary risks factors for hip fracture using a large databank (White *et al.* 2006) or by a follow-up of a large panel of subjects (Cumming *et al.* 1995, Cheng *et al.* 2009). By statistical evaluation of risk factors related to occurrence of hip fracture, they were able to determine the effect of specific factors (drug therapy, high coffee intake, tobacco smoking, neuromuscular disorder, etc.). Subjects, especially ageing females, with cumulative multiple risk factors, are the most likely to be affected by a hip fracture. Based on these studies, preventive measures such as quitting smoking, exercising and reducing caffeine intake can be recommended to people with low bone mineral density to decrease their general fracture risk (White *et al.* 2006). Recently it was shown that femoral neck and trochanteric hip fractures have different clinical risk factors (Jokinen *et al.* 2010). Specifically, low leisure-time

physical activity was a risk factor for cervical hip fractures, while high coffee consumption and low mobility were associated with increased risk of trochanteric hip fracture.

Geometrical and structural risk factors

It has been shown that both geometry and structure of the hip are essential in identification of patients at risk (Gregory *et al.* 2004a, 2007). The shape of the femoral head has been defined to be an important determinant of fracture risk (Baker-LePain *et al.* 2011); the main reason is its impact on the distribution of mechanical load during an impact (Gregory *et al.* 2008). It has been assumed that an increase in risk of fracture is proportional to the decrease of BMD at any site (Marshall *et al.* 1996), but a large multicentre study revealed that BMD alone was not a predictor of fractures (Kaptoge *et al.* 2005).

In their study, Voo *et al.* (2004) used 3D finite element models with different geometry to demonstrate that certain geometric features are significant risk factors for femoral neck stress fracture. By using the same fixed material properties in his models, they were able to study the impact of geometry itself. It has also been shown by X-ray measurements that femoral neck length is closely associated with hip fracture, independently of BMD (Bergot *et al.* 2002).

It has been reported that the distribution of fracture type is related to some specific geometric measurements of the upper femur. Cervical fractures have been shown to occur more often in patients with high NSA and thin cortex, whereas trochanteric fractures are more related to decreased BMD (Partanen *et al.* 2001, Pulkkinen *et al.* 2006, Pulkkinen *et al.* 2010).

However, both geometrical and structural parameters differ between genders as does their relevance for predicting hip fracture risk (Cody *et al.* 2000, Lochmüller *et al.* 2002, Bergot *et al.* 2002, Duan *et al.* 2003). Occurrence of cervical fracture is higher for females, resulting in fractures with lower loads (Pulkkinen *et al.* 2006).

Fall-related aspects

Falls have shown to be the primary reason for the occurrence of hip fracture (Grisso *et al.* 1991a, Geusens *et al.* 2002). Ageing increase the rates of falls due to factors such as decrease in vision, mental disorders, loss of permanent attention, and other diseases related to high age.

It is trivial to assume that the fracture occurs when the load applied exceeds the bone strength (Currey 2001, Bousson *et al.* 2011). However, the bone is adapted to usual, not to unusual loading environment. Thus, a fall will involve an unusual load intensity and direction, resulting in an increased risk of fracture (Pinilla *et al.* 1996, Currey 2003a, Sievänen & Kannus 2007). It has recently been suggested that practicing martial arts involving fall techniques might be a solution to reduce the impact forces occurring during a fall as well as the fear of falling (Weerdesteyn *et al.* 2008, Groen *et al.* 2010).

2.2.4 Experimental testing of hip failure load

In order to evaluate the strength of the bone, different mechanical tests have been developed to simulate real-time fracture using *in vitro* material. The mechanical testing of the upper femur can be divided into two groups: axial loading simulating the stand loading situation, and lateral loading simulating a fall to the side, the latter being considered the main reason of hip fracture (Lotz *et al.* 1991a, 1991b) (Fig. 4).

Axial loading of the femur

In the axial loading configuration, hip strength is measured by applying a vertical load parallel to the shaft axis (Fig. 4A). After fixation of the shaft vertically, a load is applied either on top of the femoral head parallel to the shaft axis (Beck *et al.* 1990, Eckstein *et al.* 2002, Lochmuller *et al.* 2002, 2003, Duchemin *et al.* 2008) or on the superiomedial area (rotation of 10–15° from the vertical axis) of the femoral head to simulate the load applied during the stance phase of gait (Lang *et al.* 1997, Keyak *et al.* 1998, Cody *et al.* 1999, Keyak *et al.* 2001).

Lateral loading simulating a fall

A mechanical test simulating the primary occurrence of hip fracture can be performed by applying a load on the greater trochanter while the femoral head is fixed or vice versa (Courtney *et al.* 1994, 1995, Lang *et al.* 1997, Eckstein *et al.* 2002, Lochmüller 2002, 2003, Eckstein *et al.* 2004) (Fig. 4B). The direction of the applied load is amplified by a longer moment arm (high NSA with long femoral neck axis length) (Wang *et al.* 2009). For this simulation, the shaft is typically positioned at 10° from horizontal axis and the neck at 15° of internal

rotation. The load is applied on the greater trochanter, generally through a pad. The reproducibility of such an experiment has been evaluated previously, using the contralateral femora as control, the RMS CV of repeated measures being 15% (Eckstein *et al.* 2004).

Keyak *et al.* (1998) used an internal rotation along the shaft axis of 30° and an angle between the horizontal plane vs. neck axis of 20°. In this setup, the force is applied on an area of the proximal anterior femoral head while the bone is fixed on the shaft area and the lowest part of the greater trochanter (Fig. 4B). This configuration simulates an oblique fall backward and to the side. Due to occurrence of lowest fracture loads, this configuration has been considered the most severe scenario (Lotz *et al.* 1991a, Keyak *et al.* 2001, Bessho *et al.* 2004, Wakao *et al.* 2009).

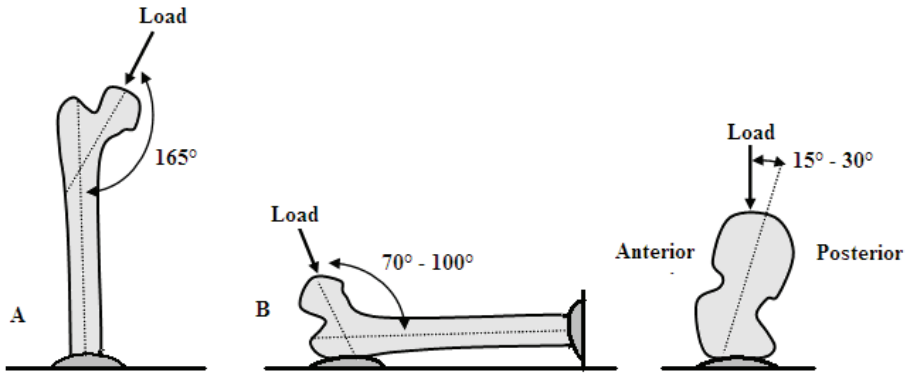

Fig. 4. Experimental testing of failure load. (A) axial loading and (B) lateral loading.

2.3 Radiological methods for the assessment of hip fracture risk and failure load

Different methods have been developed with the goal of assessing fracture risk from radiological pictures. These methods are based on the analysis of geometry, trabecular structure, mineral density or the combination of multiple parameters.

2.3.1 Radiographs

A method to assess fracture risk is indirectly related to the mineral density of the trabecular bone. The Singh index is a method to assess the resorption of trabecular loss in the upper femur by identification of the patterns of the main compressive and tensile systems (Singh 1970). The visual characterization of the five main groups of trabeculae allows some estimation of the osteoporotic level of the bone and consequently some evaluation of the fracture risk.

A similar approach has been developed to avoid relying on the human eye for the consistency of computerized evaluation of the radiographic texture pattern of bone images. Radiographic texture analysis (RTA) is a method allowing the assessment of bone architecture, as a determinant of bone quality instead of bone quantity (Vokes *et al.* 2006, 2008). Many studies have been conducted to evaluate the trabecular bone structure (Benhamou *et al.* 2001, Chappard *et al.* 2001, Veenland *et al.* 2002, Gregory *et al.* 2004a, Chappard *et al.* 2005, Huber *et al.* 2009). Unfortunately, the variation of contrast and intensity between images due to the acquisition increases the complexity of the method. However, some recent studies applying gradient-based image processing found correlations between parameters derived from texture analysis of plain radiographs and BMD in different sites (Pulkkinen *et al.* 2008, Chappard *et al.* 2010).

Finally, it has been proven that mechanical competence (Ruff *et al.* 2006) and fracture risk (Michelotti & Clark 1999, Partanen *et al.* 2001, Szulc *et al.* 2006, Rivadeneira *et al.* 2007, Cheng *et al.* 2007, Wang *et al.* 2009, Pulkkinen *et al.* 2010, Ito *et al.* 2010) can be evaluated by geometrical measurements based on anatomical references, with good repeatability (Partanen *et al.* 2001). Briefly, by comparing patients with hip fracture and controls without fracture (Table 2), the occurrence of fracture is higher for hip with high NSA, thin cortical bone and long moment arm.

Table 2. Geometrical hip fracture predictors.

Reference	Sex	N	N controls	Hip fracture predictors
Michelotti & Clark 1999	Women	43	119	Thin cortices, higher ND
Partanen *et al.* 2001	Women	70	49	Small FSD, small TW and pelvic dimensions, High NSA, thin cortices,
Szulc *et al.* 2006 (EPIDOS cohort)	Women	65	167	Thin cortices, low CSMI
Cheng *et al.* 2007	Women	45	66	Low neck cortical thickness, large FN CSA
Rivadeneira *et al.* 2007 (Rotterdam Study)	Both	147	4659	Thin cortices, greater bone width
Wang *et al.* 2009	Both	63	57	Longer moment arm
Pulkkinen *et al.*2010	Women	57	40	High NSA, thin cortices
Ito *et al.* 2010	Women	36	36	High NSA, low cortical and trabecular CSA, thin cortices, low CSMI

With ND Neck diameter, FSD Femoral shaft diameter, TW Trochanteric width, NSA Neck-shaft angle, CSMI Cross-sectional moment of inertia, FN CSA Femoral neck cross-sectional area

2.3.2 DXA

Dual-energy X-ray absorptiometry is an imaging method that allows the assessment of bone mineral density by using two X-ray beams of different energy levels. This method is widely used for the prediction of osteoporosis and at some extent of fracture risk, BMD being related to fracture load (Huber *et al.* 2008).

Hip strength analysis (HSA) is a method combining both geometry and mass distribution assessed by DXA to generate parameters evaluating the bone strength. The parameters include predictors of hip fracture such as hip axis length (HAL), NSA, cross-sectional bone area (CSA), bone width, cross-sectional moment of inertia (CSMI), section modulus, cortical thickness, and buckling ratio. Using the HSA method, the EPOS (European Prospective Osteoporosis Study) study of Crabtree *et al.* (2002) determined by how much hip geometry data improved the identification of hip fracture, concluding that this method can be applied clinically to identify women with high risk of hip fracture.

Finally, Vokes *et al.* (2006) suggested that radiographic texture analysis method can also be applied to densitometer-generated calcaneus images from DXA picture to estimate bone fragility independently and complementary to BMD measurements and age.

2.3.3 Computed tomography

Computed tomography (CT) is a method using series of 2D X-ray images along an axis in order to generate a volume by creating consecutive 2D pictures separated by a fixed thickness. This method allows not only obtaining a volumetric representation of an object, but also assessing its volumetric density at each coordinate in the space. One advantage of CT scans is the evaluation of true trabecular bone density, whereas DXA as a planar projection method results in areal BMD values affected by the projection of both trabecular and cortical bone.

Use of CT scans to study the geometry of the hip and its relationship to the occurrence of fracture allows the evaluation of volumetric measurements (Ito *et al.* 2010). This method allows evaluating geometrical parameters that cannot be assessed with radiographs due to dimensional restriction.

Strength of bone can be evaluated using quantitative CT, which allows studying bone compartments individually (Manske *et al.* 2009). Correlation has been established between BMD assessed from QCT and experimental failure load (Bousson *et al.* 2006, Huber *et al.* 2008).

Computed tomography allows volumetric evaluation of the bone structure (Baum *et al.* 2010) as well as volumetric BMD. To assess the BMD along the bone, a calibration phantom with different known densities is scanned and the Hounsfield units corresponding to the grey levels of the scans are related to the density. After adjustments using the phantom as a reference, volumetric BMD can be evaluated directly from the Hounsfield unit of the ROI and eventually the Young's Modulus can be derived from it, as demonstrated in literature (Table 3).

Table 3. Table 3. Material properties of the trabecular bone evaluated from ash density as used in studies.

Reference	Young's Modulus (MPa)	Yield stress (MPa)
*Keyak *et al.* 1994, 2001	33,900ρash2.20 for 0 < ρ ≤ 0.27	137ρash1.88 for ρash < 0.317
Bessho *et al.* 2004, 2007, 2009	5307ρash+469 for 0.27 < ρ ≤ 0.6	114ρash1.72 for 0.317 ≤ ρash
Majumder *et al.* 2007	10,200ρash2.01 for 0.6 < ρ	
*Keller 1994	10,500ρash2.29	1.0 x1020 for ρash ≤ 0.2
Wakao *et al.* 2009		117ρash1.95 for 0.2 < ρash
Schileo *et al.* 2007		
Taddei *et al.* 2006		
*Morgan *et al.* 2001, 2003	15,010ρapp2.18 for greater	85.5ρapp2.26 for greater trochanter
Schileo *et al.* 2007	trochanter	38.5ρapp1.48 for femoral neck
	6,850ρapp1.49 for femoral neck	
*Carter & Hayes 1977	3,790ρapp3	68 ρapp2
Schileo *et al.* 2007		
*Rice *et al.* 1988	900 ρapp2+60	32.66 ρapp2+2.45

*Original studies establishing the relationships

$\rho_{ash}/\ \rho_{app}$ = 0.6 (Schileo *et al.* 2007).

ρ_{ash} = 0.551 ρ_{app} (Keyak *et al.* 1994)

2.4 Finite element method

This computational method allows the estimation of mechanical behaviours of an object using information concerning its shape, structure and material properties. Briefly, the geometry of an object is divided into small parts called finite elements, considered a mathematical representation of the physical problem. Material properties as well as boundary conditions are then applied to the model to simulate an event, and the analysis of the problem is performed by solving partial differential equations. Finite element (FE) modelling has appeared to provide opportunities for estimating stress and strain distribution during simulation of various mechanical loading conditions. Application in biomechanics allows the assessment of fracture risk from models derived from different medical imaging modalities.

2.4.1 Theoretical Background

The force-deformation curve (Fig. 5) represents the behaviour of the bone mechanical properties when a load is applied. When the load increases, the deformation Δl is linear until it reaches a yield point corresponding to the limits of

the force F_{yield} that can be applied without damage. If the force applied increases above this limit, deformation becomes irreversible and eventually a force F_{max} will be reached corresponding to the failure load of the bone.

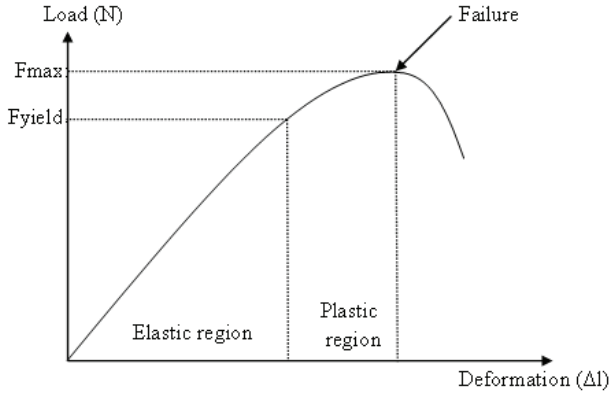

Fig. 5. Typical load-deformation curve resulting from biomechanical testing of a bone.

The FE method divides geometry into small finite segments assembled together to keep the equilibrium of the model. The method will study the displacement related to the material properties of the elements under a certain load to find a solution of the behaviours of the whole geometry. The stress corresponds to the force F applied on an area A.

$$\sigma = \frac{F}{A} \tag{2}$$

However, this formulation presumes that the stress is uniform along the area, an approximation that cannot be assumed for large areas. The discretization of geometry into finite elements allows considering small areas δA carrying smaller intensity of force δF, called ”stress at a point”:

$$\sigma = \lim_{\delta A \to 0} \left(\frac{\delta F}{\delta A} \right) \tag{3}$$

The stress matrix [σ] is the representation of the stress components in space (Fig. 6); if Cartesian coordinates are used, six components out of nine are considered (due to interchangeability).

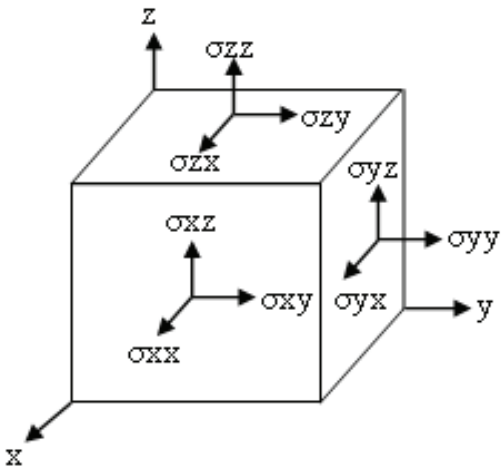

Fig. 6. Three-dimensional Cartesian stresses.

The stress matrix is represented by the three principal stress components (σxx, σyy, σzz) and the three shear stress components (σxy, σxz, σyz). Similarly to the stress matrix, a strain matrix [ε] is defined, the strain ε corresponding to the deformation Δl from the original length l:

$$\varepsilon = \frac{\Delta l}{l} \tag{4}$$

For linear elastic material, the relationship between the stress and the strain is defined by Hooke's law, defined as (if thermal strain is neglected):

$$
\begin{aligned}
\varepsilon_{xx} &= \frac{1}{E}\left[\sigma_{xx} - \nu\left(\sigma_{yy} + \sigma_{zz}\right)\right] \\
\varepsilon_{yy} &= \frac{1}{E}\left[\sigma_{yy} - \nu\left(\sigma_{xx} + \sigma_{zz}\right)\right] \\
\varepsilon_{zz} &= \frac{1}{E}\left[\sigma_{zz} - \nu\left(\sigma_{xx} + \sigma_{yy}\right)\right] \\
\varepsilon_{zy} &= \frac{1}{2\mu}\sigma_{xy} \\
\varepsilon_{xz} &= \frac{1}{2\mu}\sigma_{xz} \\
\varepsilon_{yz} &= \frac{1}{2\mu}\sigma_{yz}
\end{aligned}
\tag{5}
$$

with E being Young's Modulus (N/m²), ν Poisson's ratio and μ the shear modulus (N/m²). The relationship between E and μ for an isotropic material is defined as:

$$\mu = \frac{E}{2\left(1+\nu\right)} \tag{6}$$

For simplification, the terms on the right are grouped into an "elastic property matrix" [D], and the generalized relationship between stress and strain becomes:

$$\left[\sigma\right] = \left[D\right]\left[\varepsilon\right] \tag{7}$$

The finite element method examines the variation of stress along the elements through the whole body when the equilibrium of the forces is considered.

2.4.2 Building the model

A typical workflow for generating an FE model and performing FE analysis is presented in Fig. 7.

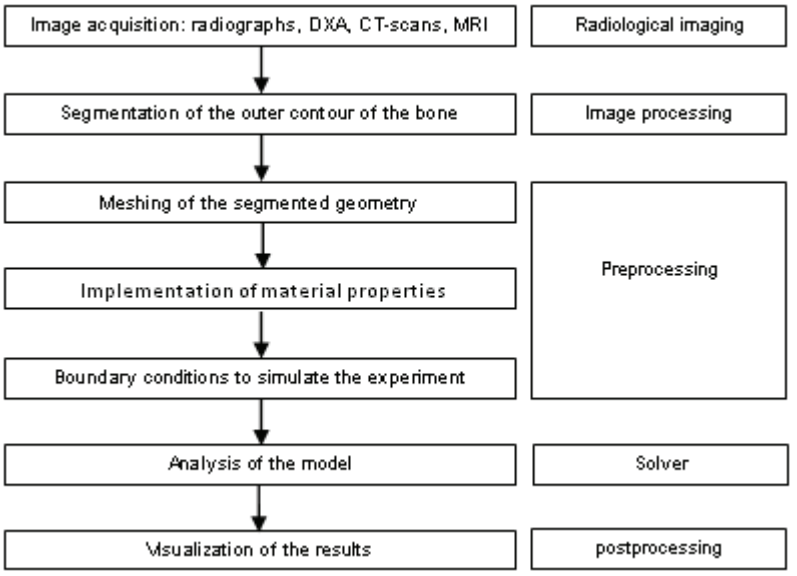

Fig. 7. Typical workflow of the finite element method process.

Segmentation of the femoral bone

To perform an FE analysis, it is required that a surface/volume be meshed to obtain a numerical representation of the model. For this purpose, the geometry of the bone is generally imported in the FE software after image processing of the original data acquisition with medical devices.

Segmentation of 2D data such as DXA and radiographs are usually performed automatically or semi-automatically using anatomical landmarks defined by the user (Testi *et al.* 1999, 2002, 2004, Yang *et al.* 2009). The outer contour of the bone is delimited and then exported to the FE software to be meshed (Fig. 8, left).

Segmentation of CT scans is typically performed manually on each slice of the volumetric data. To reduce the process, different methods such as threshold, interpolation, smoothing and shape recognition can be used. Once the segmentation is done, the volume between the segmented slices is then interpolated and the 3D model is created.

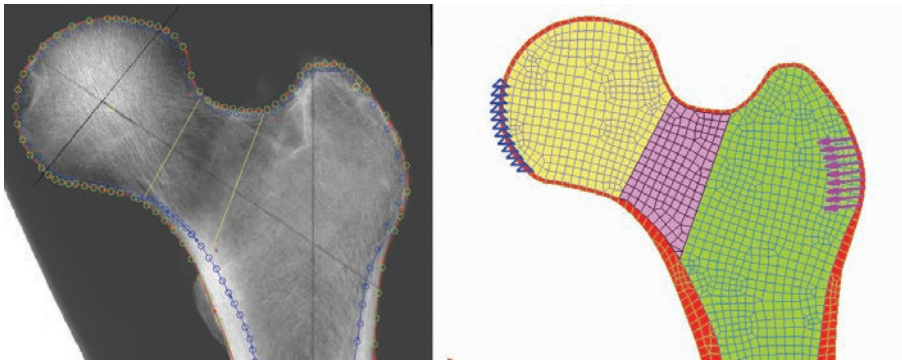

Fig. 8. Model creation from a radiographic picture: on the left, half-automatically segmented upper femur; on the right: meshed model with different material properties per area and boundary conditions. The blue triangles represent horizontally fixed nodes, allowing vertical translation, the pink arrows correspond to the location and orientation of the load applied.

Meshing

The meshing process is the subdivision of the original geometry into elements with their corners called nodes. The nodes correspond to a point in the space defined to approach the geometry. Depending on the size of the mesh, the accuracy to approximate the original shape will vary. Elements can be of different shapes. In 2D models they are generally triangles or quads (Fig. 8, right) whereas in 3D models they are tetrahedrons or hexahedrons. The meshing can use mapped algorithm for high accuracy of solids and surfaces with specific geometry, but for complex shapes, free-mesh algorithms are usually performed to reduce the processing time. After meshing, it is important to check the validity of the model to avoid any distorted/flat elements that could affect the final result of the analysis.

Material properties

Material properties in finite element method can be anisotropic, orthotropic or isotropic along the models, but to avoid complexity and computational time, most of the studies in literature use isotropic models. Even though bone material has been recognized as an orthotropic material, building such models involves extra work in the implementation of material properties (Wirtz *et al.* 2003), and only

small differences have been reported after comparison using both isotropic and orthotropic properties (Peng *et al.* 2006).

If not homogenous, the material properties have been derived from the BMD values from DXA (Testi *et al.* 1999, 2002, 2004), or Hounsfield units from CT (Carter & Hayes 1977, Keller 1994, Keyak *et al.* 1994, Morgan *et al.* 2003). Relationships have been established between these parameters and actual experiments on bones (Schileo *et al.* 2007). Typically, Poisson ratio is fixed, with a value between 0.2 and 0.4 (Wirtz *et al.* 2000, Schileo *et al.* 2007, Keyak *et al.* 1998, Ota *et al.* 1999).

Boundary conditions

The boundary conditions allow the simulation of different experiments. They are mainly defined from the conditions occurring in real life or during a specific experiment; they correspond to the degree of freedom of the model. To establish these conditions, it is possible to fix the nodes of elements totally, to allow their translation or rotation along defined axis, to simulate connections between surfaces, etc. The load can be defined on specific elements with different parameters (direction, intensity, speed of loading, etc.). The boundary conditions will characterize the behaviour of the model in space.

Solving the problem

The role of the solver is to find a solution of the partial differential equations in order to extract the nodal displacement which is the same for every element connected to it. From the displacement, the strain can be calculated, and finally, the stresses defined from the stress-strain relationships.

Post-processing

The post-processing is the investigation of the results of the analysis of the solved model. After verification of eventual errors that could have occurred during the solving process, the model is ready to be checked. Depending on the purpose of the simulation, different parameters can be displayed, such as displacement of the elements, distribution and magnitude of the stress and strain, or the failure of elements.

2.5 Evaluation of hip fracture type and failure load using finite element analysis

A sample of FE studies estimating hip fracture type or failure load is overviewed in Table 4. It has been demonstrated that femoral strength is better predicted by finite element models than quantitative computed tomography or DXA (Cody *et al.* 1999).

2.6 Creation of 3D models from 2D data

3D FE models derived from 3D imaging allow making accurate simulation of physiological situation. However, building such models requires time and use of complex imaging techniques that involve high cost and high radiation levels in most of the cases (e.g. CT or peripheral quantitative CT). One alternative to generate 3D models is to build them from 2D pictures with better time- and cost-efficiency (Gunay *et al.* 2007). The challenging part of this method is the complexity of the hip geometry and the lack of information of the 3rd axis.

2.6.1 Active shape modelling

Active shape modelling (ASM) is a method that allows an original 3D object - used as a reference/template - to deform itself in order to fit a 2D contour as an input. The ASM method will iterate processes such as rotating, scaling, translating and shaping the initial 3D model to fit the 2D contour with the best accuracy possible (Sadowsky *et al.* 2006, 2007, Gregory *et al.* 2007, Galibarov *et al.* 2010, Zheng 2010, Väänänen *et al.* 2010). For this purpose, different methods can be used, some studies using individual segmented femur from QCT (Ahmad *et al.* 2010) in order to create an atlas and to derive an averaged 3D model from it. The model is projected to 2D, and the ASM fits the projection with the original DXA picture. After the variation between both simulated 2D model and DXA picture is minimized, the 3D model is obtained by using deformation fields for the 3rd axis. Typically, the studies use DXA pictures as an input in order to obtain BMD, and eventually material properties from it.

Table 4. Finite element studies involving different techniques and aims.

Reference	N	2D/3D	Material properties	Simulation	Criteria for the goal	Goal of the study
Testi *et al.* 1999	12	2D	Derived from DXA	Fall on trochanter	Maximal principal tensile strain close/higher than ultimate strain	Predictive index of fracture risk
Yang *et al.* 2009	120	2D	Derived from DXA	Fall on trochanter	Index of fracture risk	Fracture type discrimination
Keyak *et al.* 2001	4	3D	Derived from ash density from CT	Atraumatic loading / fall with postolatearal loading	15 contiguous non-surface element failing	Effect of direction on the femoral fracture load
Schileo *et al.* 2007	4 pairs	3D	Derived from CT	Stance loading	Principal strain	Evaluation of the best density-elasticity relationship
Majumder *et al.* 2007	1	3D	Derived from CT	Sideway fall	Principal strain	Simulation of pelvis/femur with whole body representation
Bessho *et al.* 2007	11	3D	Derived from CT	Quasi-static uniaxial compressive load	Principal strain	Comparison of yield loads, fracture loads and principal strains to experiment
Qian *et al.* 2009	6	3D	Derived from DXA with 3D correspondence	Stance loading	Von Mises stress	Influence of NSA in the stress distribution
Bryan *et al.* 2009	1000	3D	Stat model from CT	Oblique fall backwards and to the side	Exceeding yield strain 0.7%	Discrimination of factors at risk
Langton *et al.* 2009a	18	3D	Derived from 2D BMD image (ash density)	Stance loading	Stiffness derived from the displacement of the loading plate	Failure load assessment from 3D model derived from 2D BMD image

ASM can also be used to quantify variations in the shape of the hip, or mode scores, on a long-term basis to discriminate patients at risk for osteoarthritis (Gregory *et al.* 2007). These mode scores have been compared to composite average proximal femur shape in order to predict osteoporotic hip fracture (Gregory *et al.* 2004, Baker-LePain *et al.* 2010).

Volumetric DXA (VXA) method uses the ASM to reconstruct a 3D model from four DXA images in different projections. Not only the geometry is generated, but the method also offers an approach to the volumetric structure derived from the DXA. In their study, Ahmad *et al.* (2010) found good correlation between the estimated volumetric BMD (vBMD) derived with the VXA method with the one obtained from QCT.

2.6.2 Statistical shape modelling

As an alternative to the ASM method, the statistical shape modelling (SSM) method allows the reconstruction of anatomical structure such as bones from sparse data. To elaborate such a tool, correspondence between each model has to be established. To summarize, a specific point in a model has an equivalent point in every model, and this concerns both the geometrical location and the material property related to it.

In their studies, Bryan *et al.* (2009, 2010) used SSM to generate 1,000 femur models with different realistic parameters representative of interpatient variability. They tested their models in a simulation of an oblique fall to the side to estimate the models with the highest risk of fracture. Based on a deeper analysis, they concluded that the main difference between failed and non-failed groups was the percentage of cortical bone.

Using correspondences between landmarks from two X-ray radiographs and 2D/3D reconstruction process of their SSM algorithms, Zheng & Schumann (2009) and Schumann *et al.* (2010) were able to generate geometrical patient-based models. Instead of validating their method by calculating the distance error between the reconstructed surfaces and the original truth surfaces, they compared clinically relevant morphometric parameters. By showing no significant difference between morphometric parameters of normal and outlier bones, they concluded that their technique was able to reconstruct both normal and outlier bones.

3 Purpose of the study

The present study examines new computational approaches to predict fracture risk by simulations of a fall on the greater trochanter. The general purpose of this study was to assess hip fracture type and failure load using radiological images and finite element modelling. The specific aims were:

1. To evaluate the structural differences between bilateral hips and their impact on the fracture type obtained during an experimental fall on the greater trochanter.
2. To investigate whether the type of fracture (cervical or trochanteric) can be accurately predicted using a 2D model of the proximal femur, generated from a standard radiograph.
3. To investigate whether the strain distribution within the upper femur coincides with the occurrence of experimental hip fracture type using a 3D model of the proximal femur, generated from computed tomography images.
4. To develop a new automatic method to generate 3D finite element model of the upper femur from a standard 2D radiograph.

4 Material and methods

4.1 Subjects

The materials and methods used in the sub-studies are summarized in Table 5. The study sample consisted of cadaver femora obtained from a larger experimental study (Pulkkinen *et al.* 2006, Eckstein *et al.* 2004) from the Institute of Anatomy at the Ludwig Maximilians University of Munich (Germany). The femora were chosen to be representative of the elderly population of the southern part of Germany. Biopsy specimens were taken from the left iliac crest for histology in order to keep only subjects without bone diseases other than osteoporosis or osteopenia.

Table 5. Summary of the materials and methods used in the study.

Study	Material	Imaging	Method
I	112 bilateral cadaver femurs (32F, 24M)	Plain radiographs	Statistical comparison
	77 with cervical fracture (55F, 22M)	DXA	
	27 with trochanteric fracture (9F, 18M)		
	8 with shaft fracture (M)		
II	49 cadaver femurs (F)	Plain radiographs	2D finite element models
	26 with cervical fracture (F)		
	23 with trochanteric fracture (F)		
III	26 cadaver femurs (F)	CT-scans	3D finite element models
	13 with cervical fracture (F)		
	13 with trochanteric fracture (F)		
IV	14 cadaver femurs (9F, 5M)	Plain radiographs	3D finite element models
		CT-scans	

F female; M male

4.2 Measurements

To evaluate the geometry, structure and BMD of the femurs, different image acquisitions were performed on the subjects. Study I was based on geometrical parameters extracted from radiographs analysis as well as bone mineral density derived from DXA pictures. Plain radiographs were used for study II in order to define the shape of the bone and the inner and outer contour of the trabecular bone in 2D. Study III was based on analysis of CT scans in order to generate the models in 3D based on manual segmentation. Finally, study IV used a

combination of radiograph pictures to extract geometrical and architectural parameters, as well as CT scans as training material to generate 3D models.

4.2.1 Image acquisition

Radiographs (I-II, IV)

Radiographs were taken using a Faxitron X-ray system (Model 43885A; Faxitron, Hewlett Packard, McMinnville, OR, USA) at 40 to 85 kV, 2mA, time = 120s, using a 18*24cm X-ray film (Agfa Structurix D7DW, Agfa, Leverkusen, Germany), and the X-ray films were digitized together with a calibration scale using a scanner at 600dpi.

CT-scans (III-IV)

The femora were scanned with a 16-row multi-detector CT scanner (Sensation 16; Siemens Medical Solutions, Erlangen, Germany). The specimens were degassed, packed in airproof plastic bags filled within a formalin/water solution and positioned in the scanner comparable to the *in vivo* exam of the pelvis and proximal femur. A high-resolution protocol with a slice thickness of 0.75 mm was used. The settings were 120 kVp and 100 mAs, image matrix 512 x 512 pixels, and field of view of 100 mm. The in-plane spatial resolution was approximately 0.25 mm x 0.25 mm. For calibration purposes, a reference phantom (Osteo Phantom, Siemens, Erlangen, Germany) was placed below the specimens. Images were obtained in Digital Imaging and Communications in Medicine (DICOM) format for segmentation and analysis.

DXA (I)

In vitro DXA scans of the femora were obtained using a standard narrow fan beam scanner (GE Lunar Prodigy, GE Lunar Corp., Madison, WI, USA) with the femoral specimens submerged in a water bath. Standard positioning was used across all specimens, and both total and site-specific femoral BMDs were checked. The bone mineral density was evaluated in the neck area, upper neck area, shaft area and trochanteric area using the software provided by the manufacturer.

4.2.2 Geometrical parameters (I, II, IV)

To focus on the geometry on the bone and its impact on the bone strength, geometrical dimensions were assessed from the radiographs for each femur (Fig. 9).

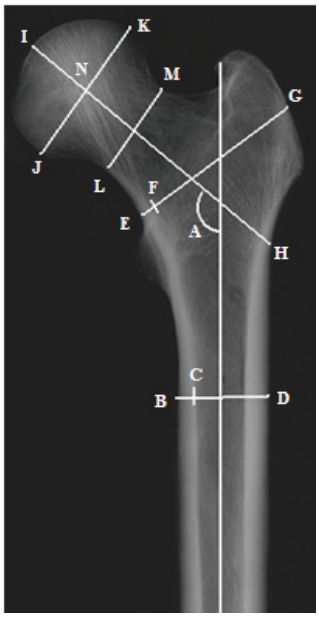

Fig. 9. Geometrical parameters measured from the radiographs of the upper femur. A, neck-shaft angle (NSA); B-D, femoral shaft diameter (FSD); E-G, trochanteric width (TW); J-K and L-M, femoral head and femoral neck diameters (HD and ND respectively); H-I and H-N, femoral neck axis length (FNALa and FNALb, respectively); B-C, femoral shaft cortex width (FSC); and E-F, medial calcar femoral cortex width (CFC).

Femoral neck axis length (defined in two ways, FNALa and FNALb); neck-shaft angle (NSA); trochanteric width (TW); femoral head (HD), neck (ND), and shaft (FSD) diameters; and femoral shaft (FSC) and calcar femoral cortical thicknesses (CFC) were measured as previously described (Partanen *et al.* 2001) using Image Tool software (version 3.00; University of Texas Health Science Center, San Antonio, TX). The root mean square coefficients of variation (CVrms) were 0.9%, 1.5%, 1.1%, 2.5%, 1.5%, 0.7%, 2.5%, 5.2%, and 9.9% for FNALa, FNALb, NSA, TW, HD, ND, FSD, FSC, and CFC, respectively (Partanen *et al.* 2001).

4.2.3 Architectural parameters derived from image processing (IV)

Image processing was performed with an algorithm developed under MATLAB (version 7.1, MathWorks, Natick, Massachusetts, USA) with a graphical interface allowing the user to select a specific region of interest (ROI) (15mm x 15mm). Image pre-processing was applied to the picture, i.e. noise was removed using a median filter and morphological top and bottom hat operations were performed. A gradient-based gray-level image was then constructed as previously described (Pulkkinen *et al.* 2008).

Fourier transform was applied to the ROI in order to evaluate the trabecular main orientation (TMO). A threshold of 0.03 was used to remove non-significant frequencies, and linear regression was applied to fit a line $g(x) = ax + b$ to extract the TMO in the frequency domain. Eventually, the angle α between the TMO and the shaft axis in the space domain was calculated from trivial trigonometry from the previous equation. A rotation of the ROI based on the angle α was performed to obtain a ROI aligned along TMO. A gray-level co-occurrence matrix GLCM was calculated along the TMO with a distance of one pixel. First column and first row were cropped from the GLCM to remove the values corresponding to empty spaces in the bone. Homogeneity index (HI), which measures the closeness of the distribution of elements near the diagonal of the GLCM, was calculated as follows:

$$HI = \sum_{i,j} \frac{GLCM(i,j)}{1+|i-j|} \tag{8}$$

Cropping the GLCM affects directly the result of the HI values by lowering them. This method was chosen in order to evaluate solely the homogeneity of the mineralized trabecular bone. For example, a picture with almost no trabecular bone will have a lot of pixels with values close to 0. As a result, its GLCM will have a very high value in the first diagonal cell, ending up with a HI close to 1. A pre-study was performed to evaluate the ROI with the best correlation with the total BMD and eventually the distribution of material properties through the principal systems themselves. The ROI with the best correlation was the lower neck area, corresponding to the highest density through the trabecular bone.

4.2.4 Mechanical testing (I-IV)

The mechanical test was performed earlier using a testing setup simulating a fall on the greater trochanter (Eckstein *et al.* 2004). The femoral shaft was positioned at 10° from horizontal axis, and neck at 15° internal rotation. Two halves of a tennis ball were used to simulate cartilage contact in the femoral head. The load was applied to the greater trochanter through a pad simulating soft tissue at a constant loading speed of 6.6 mm/second, using a material testing machine (Zwick 1445, Ulm, Germany). The failure load was defined as the maximum value of the load-deformation curve.

4.3 Generation of finite element models

For each finite element study (II-IV), the boundary conditions of the models were chosen to simulate a fall on the greater trochanter mimicking the mechanical test. Loading was applied on the greater trochanter through simulated soft tissue with an angle of 10° with the horizontal-axis and the neck with an internal rotation of 15°. The minimal cortical thickness on the proximal femur for the models was adjusted to 1 mm using shell elements, and a fixed Poisson's ratio of 0.33 was used in all studies. A summary of the finite element studies is presented in Table 6.

Table 6. Description of the finite element studies.

Study	Building method	Material properties	Mesh size	Goal and criteria
II	2D model radiograph (Semi-automatic)	Cortical: 14.2 GPa Trabecular: 780 / 300–900 MPa	Cortical: 1–2 mm Trabecular: 2 mm	Fracture type, stress distribution in trabecular bone
III	3D model CT-scans (manual)	Cortical: 15 GPa Trabecular: 1.1 Gpa	Cortical: 1–3 mm Trabecular: 3 mm	Fracture type, strain distribution in trabecular bone
IV	3D model geometrical parameters (automatic)	Cortical: 14.2 GPa Trabecular: based on structural analysis from radiographs	Cortical: 1–3 mm Trabecular: 1–3 mm	Fracture load, failing elements in cortical bone

4.3.1 2D models from radiographs (II)

After filtering of radiographs to enhance edges on the pictures, semi-automatic custom algorithms were applied to extract the cortical *vs*. trabecular bone

compartments based on grey levels using MATLAB. For each bone, two neutral files were generated:

- A model with only two Young's modulus values (one for cortical bone and one for trabecular bone).
- A model with the same Young's modulus value for cortical bone and four different values for different trabecular bone areas (900 MPa for femoral head, 780 MPa for femoral neck, 600 MPa for trochanteric region and 300 MPa for subtrochanteric region) (Wei *et al.* 2005, Sievänen *et al.* 1996, Martens *et al.* 1983), the areas separated using anatomical landmarks.

Neutral files were imported into Femap (Finite Element Modeling and Postprocessing, version 9.2.0, UGS Corp., Plano, TX, USA) software used for the pre- and post-processing of images and boundary conditions were applied to the models. Due to spatial restrictions, the internal rotation of the bone used in the experiment was ignored in this 2D study.

VonMises stress analysis was performed for each model using NASTRAN (version NX; UGS, Plano, Texas, USA). The fracture type was evaluated from VonMises stress distributions within the trabecular bone and the location of maximum continuous stress patterns.

4.3.2 3D models from computed tomography (III)

The Medical Image Processing and Visualization software MeVisLab (version 1.6, MeVis Research GmbH, Bremen, Germany) was used for the image segmentation. The two-dimensional slices of the proximal femur DICOM file set were manually segmented to cortical and trabecular bone contours, and these contours were automatically combined and converted to 3D surfaces of the trabecular and cortical bone. The stereolitographic (STL) files of the surfaces were imported in the FE modelling software. A homogenous Young's modulus of 1.1 GPa for the trabecular bone and 15 GPa for the cortical bone was applied to estimate the impact on the geometry itself on fracture type (Lengsfeld *et al.* 1998).

After strain analysis using NASTRAN, the principal strain and its distribution at the trabecular bone area were analysed along the model; seven planes parallel to the femoral neck axis with a distance of 2 mm were used to estimate the volumetric distribution. Assessment of fracture type was based on the highest threshold of uniform strain patterns over the cervical and trochanteric regions.

4.3.3 3D models from radiographs (IV)

In order to establish relationships between the geometrical parameters and the skeleton of the femurs, we used seven bones with a large range of geometrical parameters as training material. The CT data of these seven bones were manually segmented under Mimics (v12.1, Materialise, Leuven, Belgium). Segmented cortical bone models were then imported into FEMAP to obtain the accurate volumetric shape of the outer contour of the bones.

Since the geometry of the femoral neck area is considered critical (Qian *et al.* 2009), the non-circular cross-section of the femoral neck (Zebaze *et al.* 2005) was estimated by using the training material. The neck area was divided into segments along the FNAL and for each of these segments, the radius of the neck was checked in every 45° and correlated with geometrical parameters.

An algorithm based on the geometrical parameters was developed in order to minimize the geometrical error while comparing the models generated from the script with the models from the training material. Two curves representing the orientation of the principal tensile system (PTS) and principal compressive system (PCS) based on the geometry were also generated (Rudman *et al.* 2006).
A Young's modulus of 14.2GPa was assigned to the cortical bone (Viceconti *et al.* 1998). An intermediate Young's modulus of 7GPa was given to the first layer of elements from the cortical bone in order to simulate the transition between cortical and trabecular bones.

As training material, Young's moduli derived from the Hounsfield units from the CT scans were used as described previously (Duchemin *et al.* 2008a). This true volumetric measurement was assessed in different regions of the trabecular bone to represent the spatial distribution of material properties along both the PTS and the PCS. Material properties were affected with a linear increase along both PTS and PCS within an estimated consistent thickness, based on HI of the lower neck area extracted from the radiograph as described previously. An extra layer of elements with lower Young's modulus was generated to lower the transition with the elements outside the system area. The Young modulus values were linearly increasing from the greater trochanter until the femoral head area along the tensile system. In PCS, the highest Young's modulus values were located in the lower neck and the lowest values in the upper part of the femoral head.

The rest elements outside PTS and PCS in the shaft, trochanteric, femoral neck, and femoral head regions, which had no material properties assigned, were grouped, and a single material property was derived from the HI for each area.

Based on these relationships, a typical distribution of Young's modulus within the generated models is presented in Fig. 10. As a result, a total of 66 material properties were created:

- the cortical bone and the transition between cortical and trabecular bone
- 4 material properties for the areas outside PTS and PCS
- 20 material properties for the tensile system and 20 for the transition layer
- 10 material properties for the compressive system and 10 for the transition layer

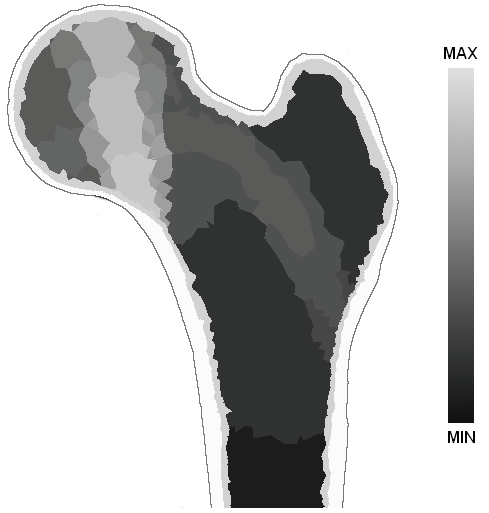

Fig. 10. Typical distribution of the material properties in a generated model, from a plane passing through the centre of the bone. The darker values correspond to elements with low-density parameters while the light values have high density. The cortical bone is represented in white, surrounded by the outer surface of the bone.

Mean reconstruction error was assessed on seven other bones by comparing the distance between the generated geometry and the original 3D finite element model derived from the CT scans. To validate the methodology, a preliminary finite element analysis simulating a fall on the greater trochanter, as described above, was performed on seven femur models generated from the algorithm. After applying boundary conditions to simulate the experiment, nonlinear FE analysis was performed using the Newton-Raphson method and Drucker-Prager yield criterion (Drucker & Prager 1952), a post-yield modulus 5% of the Young modulus was used (Bayraktar *et al.* 2004) and the ultimate tensile stress was presumed to be 0.8 times the compressive yield stress (Bessho *et al.* 2007). The

fracture was determined to occur when a surface cortical element failed (Bessho *et al.* 2007), failure in tension being characterized by a maximum principal stress higher than the ultimate tensile stress and failure in compression by a minimum principal strain lower than −7300 microstrain.

4.4 Statistical methods (I-IV)

For each study, statistical analyses were performed using SPSS statistical software (version 16.0; SPSS, Chicago, IL). For all studies, a p-value smaller than 0.05 was considered statistically significant.

Student's paired t-test was used to evaluate bilateral asymmetries in study I. For further intrasubject analysis, femurs were grouped by their experimental fracture type and pair-wised analysis using the Wilcoxon signed rank test was performed between the sides. This method was chosen due to the small sample size in order to test the differences in the parameters between cervically fractured femurs and their contralateral sides with trochanteric fractures. Finally, an intersubject analysis was performed to compare asymmetric fracture cases with symmetric ones using Student's independent t-test. A similar statistical method was used in study II, grouping being done by fracture type only.

In order to determine the best combination of geometrical parameters for the prediction of fracture type and to compare their ability to discriminate it with the FE method, a logistic regression analysis was performed in study II. Regression analysis was used in study IV to establish a relationship between the distribution of Young's modulus derived from Hounsfield units in CT scans and structural parameters assessed from image analysis of plain radiographs.

In study III, a Mann-Whitney test was performed to compare the cervical/trochanteric principal strain threshold ratio from the FE analysis with the actual, experimentally obtained fracture type. A covariance analysis (ANCOVA) using BMD as covariate was also performed to show the independence of the fracture type from the mineral density. Finally, to assess the ability of the method to discriminate the fracture type, both specificity and sensitivity were tested using a receiver operating characteristic curve (ROC) analysis.

5 Results

5.1 Bilateral asymmetries in fracture types (I)

The distribution of bilateral fractures types is presented in Table 7. The distribution of fracture type did not show any tendency for a side-related specific fracture; both cervical and trochanteric fractures occurred on left and right side. Thus, we decided to perform a left-right comparison by gender and then with all subjects pooled together to show that the eventual asymmetries are not related to the fracture type.

Table 7. Distribution of samples by different fracture types occurring during the mechanical test.

Gender	C/C	C/T	T/C	T/S	S/T	T/T
Females	46	9	9	-	-	-
Males	14	8	8	8	8	2

C cervical, T trochanteric, S shaft

5.1.1 Asymmetries between the left side and right side

Similar asymmetries were found between males and females while comparing geometrical parameters and BMD of both sides. For both genders, the cortical bone was thicker on the right femur ($p < 0.01$) and the FSD larger ($p < 0.01$), whereas HD ($p < 0.001$) and ND ($p < 0.05$) were smaller. FNAL differed between the left and right side only in males ($p < 0.01$), being higher on the left side. No significant difference between sides was found in BMD.

5.1.2 Asymmetries related to fracture type

Results for intra- and inter-subject analysis are presented in Table 8. The intra-subject analysis was performed between the cervically fractured side of an individual versus the contralateral side with trochanteric fracture. A pre-study showed no statistically significant differences between a femur with a trochanteric fracture versus its contralateral side with shaft fracture. For this reason, and due to restricted sample size, we decided to pool both trochanteric and shaft fractures together for the inter-subject analysis.

Table 8. Structural parameters, failure load and upper femoral neck BMD (UFnBMD) vs. fracture type of the femur in question and its contralateral counterpart.

Gender	Type	N	NSA	FSC	CFC	FNALa	FNALb	HD	ND	TW	FSD	HD/ND	load	UFnBMD
Females	C/C	46	127,4+++	0.49	0.40	9.72+	7.61	4.51+	3.02	5.86	3.07	1.50++	2838	0.46
	C/T	9	121.7	0.48	0.40	9.46	7.65	4.34	3.04	5.83	2.98	1.43	2996	0.44
	T/C	9	118.8(*)	0.51	0.43	9.44	7.56	4.41	3.01	5.78	3.04	1.47*	3142	0.44
Males	C/C	14	125.1	0.60	0.49	10.69	8.53+	5.02++	3.50	6.34+	3.28+	1.44	4467	0.51++
	C/T	8	126.9	0.63	0.51	11.12	8.89	5.38	3.60	6.62	3.43	1.50	4877	0.61
	T/C	8	127.4	0.56	0.45	11.12	9.02	5.29*	3.62	6.75	3.50*	1.47	4916	0.58
	T&S	18	122.1	0.61	0.51	10.76	8.57#	5.10#	3.54	6.48	3.32	1.44	5968##	0.72##

(*)$p < 0.1$; * $p < 0.05$, asymmetrical cervical fracture cases (C/T) vs. their contralateral trochanteric fractures (T/C).

+$p < 0.05$; ++$p < 0.01$; +++$p < 0.001$, symmetrical cervical fracture cases (C/C) vs. asymmetrical fractures (C/T and T/C).

(#)$p < 0.1$; #$p < 0.05$; ##$p < 0.01$, trochanteric/shaft (T&S = T/S, S/T and T/T combined) fracture cases vs. asymmetrical fractures (C/T and T/C).

Differences within subjects with asymmetric fractures

In intra-subject analysis of females, NSA showed a tendency to be lower in asymmetric trochanteric fractures (T/C) than their contralateral sides ($p = 0.066$). The T/C cases also presented higher HD/ND ratio than C/T ($p < 0.05$). In males, the trochanteric side had a lower HD ($p < 0.05$) and higher FSD ($p < 0.05$) than its contralateral C/T side. No differences were found in BMD or fracture load within these subjects.

Differences between subjects with asymmetric and symmetric fracture types

The inter-subject analysis of females showed that the symmetrical cervical (C/C) cases had significantly higher NSA ($p < 0.001$) than those with asymmetric fracture type (C/T and T/C). C/C cases also had higher HD ($p < 0.05$), implying higher HD/ND ratio ($p < 0.01$). Finally, FNALa ($p < 0.05$) was lower for asymmetrical fracture types for a similar FNALb. No significant differences in BMD were found between the groups.

In males, the subjects with asymmetric fractures (C/T and T/C) showed larger dimensions when compared with C/C cases ($p < 0.05$ to $p < 0.01$), and also when compared with all other subjects combined together (T&S = T/T, T/S, S/T) ($p < 0.05$). They also had a higher NSA ($p < 0.05$) than the T&S cases. BMD was the smallest for bilateral cervical cases.

The experimental failure load showed an increasing trend from symmetric cervical cases to asymmetric cases towards bilateral trochanteric cases (T&S).

5.2 Prediction of experimental fracture type (II-IV)

The prediction of fracture type in studies II and III was done using FE analysis, with main focus on the geometry. Thus, the material properties were similar for each bone. Accuracy of each method to predict the fracture type is presented in Fig. 11. Due to a limited sample size, accuracy was not evaluated for study IV. However, the fracture type was directly predicted from the localization of the failing element on the surface of the cortical bone.

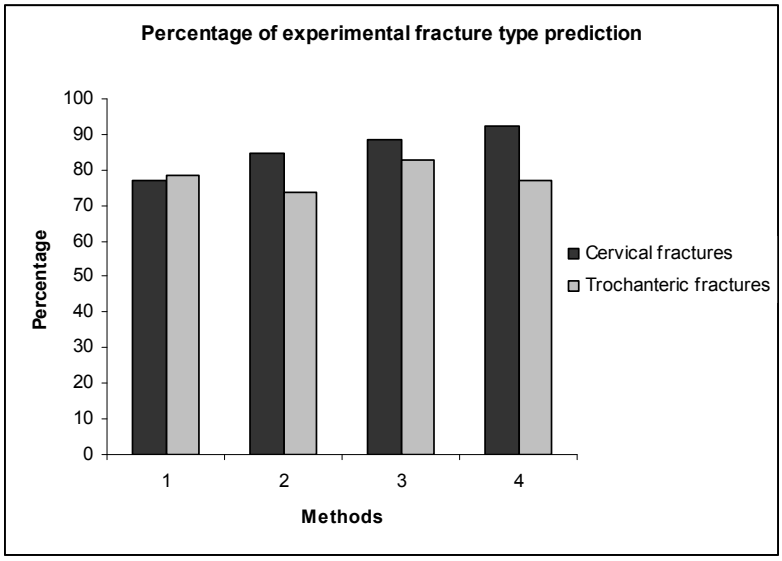

Fig. 11. Accuracy of fracture type prediction in percentage: (1) Geometrical parameters, (2) 2D FE (homogeneous trabecular bone), (3) 2D FE (heterogeneous trabecular bone), and (4) 3D FE.

5.2.1 2D models to assess fracture type (II)

To assess fracture type, VonMises stress distributions within the trabecular bone were evaluated and the regions of maximum continuous stress patterns were

determined. Two different criteria were defined: (1) location of the peak stress value and (2) region of the maximum continuous stress pattern (Voo *et al.* 2004).

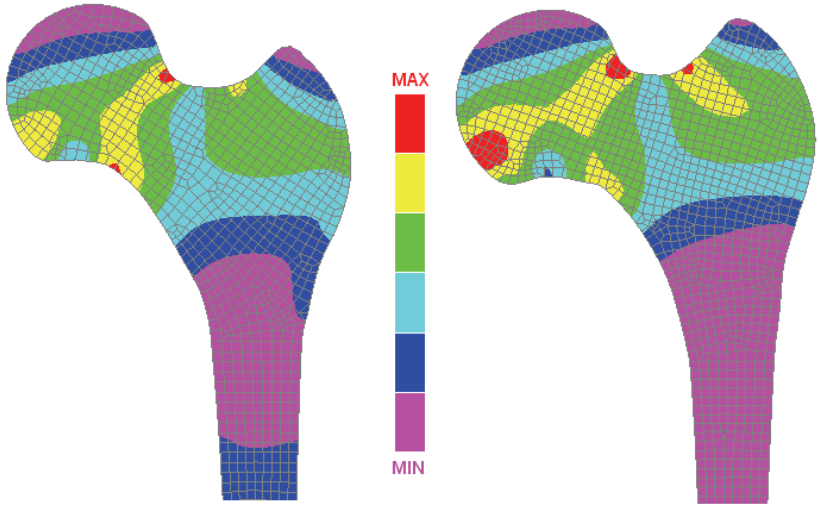

Fig. 12. Typical Von Mises stress distribution for a specific fracture type: on the left, cervical fracture: on the right, trochanteric fracture. MIN/MAX refer to minimum and maximum VonMises stress values for each bone.

This procedure predicted the fracture type correctly in 79.6% of the cases using the models with homogeneous trabecular bone properties. A slight improvement in fracture type prediction was achieved by using the models with 4 different material properties for the trabecular bone. Here, 85.7% of all cases were predicted correctly.

Both finite element analyses showed better fracture type prediction than the analysis of the best combination of geometrical predictors, these being the NSA and the femoral neck axis length, with accuracy of 77.6%. The best criterion for the prediction of hip fracture type from FE analysis is shown in the decision-making tree (Study II, Fig. 4). Briefly, to be predicted as a cervical fracture, the maximum VonMises stress has to be located in the neck area and the stress pattern through the neck; otherwise, the fracture type is considered trochanteric (Fig. 12).

5.2.2 3D strain distribution to assess fracture type (III)

The highest threshold for uniform strain patterns differed significantly between cervical and trochanteric fractures ($p = 0.001$). Experimental cervical fractures showed a cervical/trochanteric principal strain threshold ratio $\varepsilon_C/\varepsilon_T$ to be higher (1.103 ± 0.127) than in trochanteric fractures (0.925 ± 0.137) ($p = 0.001$). Using the cut-off value of $\varepsilon_C/\varepsilon_T = 1.0$ as criterion, FE model predicted the experimental fracture type correctly in 85% of the cases (12/13 cervical; 10/13 trochanteric fractures). The result appeared to be independent of BMD, since the difference remained significant after adjustment for FNBMD and TRBMD ($p = 0.014$).

5.3 Generating a 3D finite element model from a radiograph (IV)

Precision of the shape reconstruction from a radiograph was assessed by comparing the generated 3D shape with its corresponding 3D model constructed from segmented CT scans. The mean shape error for the seven bones per area is shown in Table 9; the mean error being 1.77 mm ± 1.17mm.

For all the bones, the maximum average error is located in the trochanteric area while the minimum average errors are located in the femoral head and the neck areas (1.03 mm ± 0.45 mm and 1.27 mm ± 0.60 mm, respectively). The average error in the femoral head is mostly due to the spherical approximation of the femoral head, the maximum error being located in the excavation of the *fovea capitis* where the ligaments of the *acetabulum* are attached.

Table 9. Mean shape error in mm (± SD).

Bone ID	Femoral head	Femoral neck	Trochanteric area	Shaft area	Total
1	0.97 (0.39)	1.19 (0.50)	2.17(1.15)	1.39 (0.60)	1.70 (1.04)
2	1.10 (0.53)	1.19 (0.63)	2.30 (1.4)	1.59 (0.80)	1.77 (1.21)
3	0.93 (0.44)	1.16 (0.53)	2.07 (1.21)	1.61 (0.74)	1.64 (1.08)
4	1.19 (0.47)	1.47 (0.60)	2.60 (1.69)	1.58 (1.25)	2.00 (1.46)
5	1.09 (0.46)	1.40 (0.70)	2.19 (1.34)	1.48 (0.67)	1.80 (1.16)
6	0.99 (0.42)	1.31 (0.66)	2.47 (1.50)	1,58 (0.66)	1.94 (1.34)
7	1.00 (0.42)	1.17 (0.60)	1.89 (1.02)	1.80 (0.79)	1.57 (0.93)
Average	1.03 (0.45)	1.27 (0.60)	2.24 (1.33)	1.57 (0.79)	1.77 (1.17)

The relationship between the HI, assessed in the lower neck area from the cropped GLCM along the trabecular main orientation, and the neck BMD derived from DXA is presented in Fig. 13. R^2-value is 0.82 when HI is compared to the

BMD of the corresponding area and $R^2 = 0.71$ when compared with the total BMD of the bone. The HI increases linearly with the BMD when the GLCM is cropped from all the black values of the pictures.

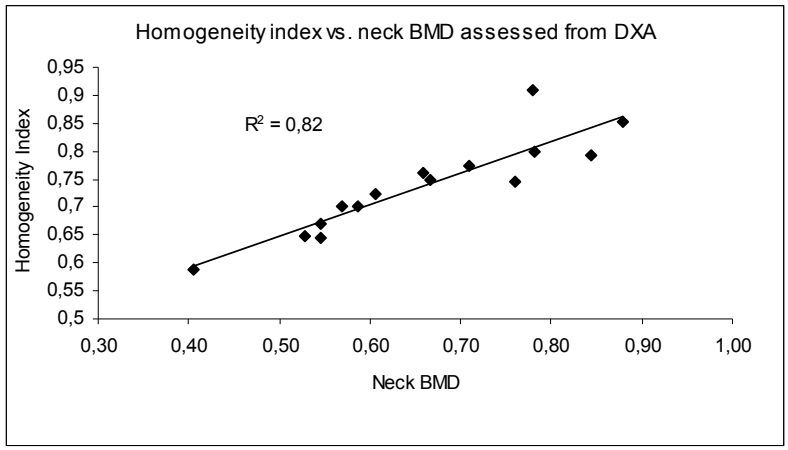

Fig. 13. Relationship between neck BMD assessed from DXA and homogeneity index (HI) derived from cropped gray-level co-occurrence matrix calculated along the trabecular main orientation. The HI is calculated from the lower neck area.

Relationships between the homogeneity index as assessed in the lower femoral neck area from radiographs, and the average Young's modulus within the compressive and tensile trabecular systems as assessed from CT-based Hounsfield units are presented in study IV (Fig. 4, page 4).

5.4 Prediction of experimental fracture load (IV)

The results for predicted failure load vs. experimental fracture load, as well as the experimental fracture type and location of the failing element in the model are presented in Table 10. Predicted failure load showed to be well-correlated with the experimentally measured load.

However, the strength of bone 5 being highly under-estimated, the differences between cortical Young's modulus derived from CT scans and the one used in our models (14.2 GPa) was evaluated. While all the bones showed a close value for the Young's modulus of the cortex (217 MPa ± 130 MPa), the cortical bone of bone 5 was highly underestimated, being 15.3 GPa in the original CT model.

Table 10. Experimental fracture load and type vs. predicted failure load and location of the failing elements.

Bone ID	Experimental load [N]	Predicted load [N]	Experimental fracture type	Location of failing element
1	1718	1680	Cervical	Femoral head - neck
2	2952	3375	Cervical	Femoral neck
3	3533	3168	Cervical	Femoral neck
4	2351	2569	Cervical	Femoral neck- trochanter
5	4536	3705	Trochanteric	Trochanteric area
6	2842	3474	Trochanteric	Trochanteric area
7	3635	3802	Trochanteric	Femoral neck

The location of the failing element was also compared to the experimentally obtained fracture type (Table 10). In five out of the seven bones, the failing elements were located in the corresponding area, in the femoral neck area for cervical fractures and in the trochanteric area for the trochanteric fractures. In bone 4, the location of the failing element was in the border line, whereas bone 7 showed a failing element in the femoral neck when the experimentally obtained fracture type was trochanteric.

6 Discussion

Hip fracture is considered the most severe fracture injury that commonly leads to devastating consequences. Most hip fractures occur after a fall, such as one from standing height, the risks factors increasing with age, as well as the level of osteoporosis (Cumming 1995). Therefore, new fall prevention strategies should be developed (Stevens & Olson 2000, Gillespie *et al.* 2009). The clinical assessment of osteoporosis, and to some extent fracture risk, is based on the BMD derived from DXA, the BMD being related to fracture load (Huber *et al.* 2008). However, it has been shown that using such a method is insufficient for predicting individual fracture risk (Schuit *et al.* 2004). This demonstrates an urgent need for more accurate tools for the assessment of osteoporotic fracture risk.

As an alternative tool, FE models have shown good accuracy as computational methods to assess the hip fracture risk (Cody *et al.* 1999). However, the complexity of accurate finite element models requires the use of more complex medical imaging technology, resulting in the use of time-consuming methods as well as increases in computational costs. To reduce these costs, one alternative is to study the capability of radiograph-based finite element models in the prediction of individual fracture risk.

6.1 Geometrical and structural influence (I, IV)

Based on Study I, it appears that a single femur has a tendency for a cervical or trochanteric fracture. Performing the analysis pairwise emphasized the impact of hip structure in the occurrence of a specific fracture type. However, the determinants of fracture type were different between genders, BMD being more important for fracture types in males whereas geometrical parameters were better predictors for females, as also suggested previously (Pulkkinen *et al.* 2004, Duboeuf *et al.* 1997)

The left-right analysis exposed different dimensions by side, the left side being typically bigger than the right one, except for the shaft diameter as previously reported (Macho 1991, Cuk *et al.* 2001, Brownbill *et al.* 2003). It is also interesting to notice that side asymmetries between males and females are the same, except for femoral axis length, which was not statistically different in females (Faulkner *et al.* 1995).

Despite the fact that the left side is considered the supportive limb (Cuk *et al.* 2001, Samaha *et al.* 2008), resulting in left-right functional asymmetries, the

experimentally obtained fractures did not show a side dominance for a specific fracture type. In fact, while grouped by fracture type, pairwise analysis showed different asymmetries than left-right analysis.

Inter-subject analysis, grouping subjects by symmetrical and asymmetrical fracture type, suggested that an individual has a structure-related tendency for a certain type of fracture. The predictors of a specific fracture type were different between males and females, being more dependent on NSA for females and BMD for males. The failure load showed an increasing trend from symmetric cervical cases to asymmetric cases and bilateral trochanteric cases, a trend that followed the BMD increase in males.

In summary, for females, high NSA and HD/ND ratio will more likely be associated with symmetric cervical fractures for a subject and will determine either a cervical fracture or a trochanteric one for asymmetrical cases. For males, the first predictor for symmetrical cervical fractures, asymmetrical fractures and symmetrical trochanteric fractures is BMD. For asymmetrical fracture type, geometry will have an effect on the tendency for a fracture, low FSD and high HD being related to cervical fractures. Symmetrical trochanteric fractures are also associated with low NSA while asymmetrical trochanteric fractures are not, demonstrating the gender-specific impact on fracture-type biomechanics.

In study IV, the distribution of material properties of the trabecular bone was derived from parameters derived from picture analysis of plain radiographs, as suggested by Pulkkinen *et al.* (2008) and Chappard *et al.* (2010). By using GLCM-based trabecular parameters, we were able to reveal the spatial distribution of gray levels. However, the typical method to ensure rotational invariance of the GLCM is to average it along four different orientations (0°, 45°, 90° and 135°). In our method we decided to calculate the GLCM along the TMO in order to emphasize the anisotropy of the trabecular bone. In addition, to reflect the true bone content inside the ROI, we cropped the first row and column of the GLCM before calculating the HI in order to remove the values related to empty spaces. A pre-evaluation of this method showed linear relationship between DXA-based BMD and the calculated HI. Furthermore, the influence of the principal trabecular systems was taken into account using the TMO for GLCM calculation, as it has been suggested that the principal orientation used in an orthotropic model should be defined from the trabecular structure (Yang *et al.* 2010).

Results from study I justify the methodology of study II and study III. The prediction of fracture type of females being the aim of these studies, FE models solely based on geometry should be sufficient for accurate prediction. However,

failure load prediction requires a more complex model involving personalized material properties, the failure load being related to the BMD (Marshall *et al.* 1996)

6.2 Finite element methodology (II-IV)

While most studies on finite element models of the upper femur are today performed in 3D, we decided to study how well a simple 2D model could predict an experimental fracture type. As has been suggested previously (Partanen *et al.* 2001, Gnudi *et al.* 2002, Pulkkinen *et al.* 2006, 2009), measurements of geometrical parameters from standard radiographs can indicate a tendency for a specific fracture type. From this statement, we hypothesized that a model based solely on the geometry derived from a standard radiograph might predict the fracture type with even better accuracy than the combination of geometrical parameters. As the cortical thickness showed to be a critical issue in the assessment of hip fracture (Partanen *et al.* 2001, Pulkkinen *et al.*2004, Szulc *et al.* 2005, Pulkkinen *et al.* 2006, Cheng *et al.* 2007, Pulkkinen *et al.* 2008, Ito *et al.* 2010), we decided to separate the trabecular and cortical compartment in the process of segmentation. We used similar homogeneous material properties in our models, roughly adjusted locally based on anatomical regions. Compared to previous studies (Testi *et al.* 1999, 2002, Yang *et al.* 2009) which used DXA to generate 2D FE models of the proximal femur, taking into account also the BMD of the bone, our models were developed to evaluate primarily the impact of the geometry. However, while DXA cannot be used to accurately identify the cortical thickness the use of standard radiographs allowed us to obtain better accuracy in the segmentation of the cortex.

In study III, 3D models generated from segmented CT scans were used. In his study, Voo *et al.* (2004) demonstrated the importance of bone geometry and especially the impact of NSA as well as the thickness of the cortical bone for the stress-strain distribution. Based on this hypothesis, we decided to correlate the strain distribution with a typical fracture type obtained experimentally. Similarly as in study II, both bone compartments were segmented and homogeneous material properties were assigned to them. In support of this methodology, Holzer *et al.* (2009) demonstrated that the relative contribution of trabecular bone is marginal for bone strength when compared to the contribution of cortical bone, explaining only 7% of fracture load. However, a study by Manske *et al.* (2009)

showed opposite results as they concluded that both cortical and trabecular bone affect the failure load.

The methodology used in study IV may offer an alternative to the ASM method. One of the main advantages here is the separation of bone compartments. The heterogeneous distribution of material properties was determined using the homogeneity index and the localization of principal trabecular systems. The correlation between the homogeneity index and bone mineral density (Fig. 13) showed opposite results when compared to the previously published method, since zero values originated from the bone marrow dominate in the uncropped GLCM (Pulkkinen *et al.* 2008). This method is fundamentally different from the method typically used in ASM, where material properties are directly derived from the DXA-based BMD. As a result, the generation of a model was totally automated, using geometrical parameters with high repeatability as an input (Partanen *et al.* 2001) for the shape of the bone and the homogeneity index for an estimation of the material properties.

Study II and study III used a protocol that ignores the real distribution of material properties through the bone in order to focus on the impact of the geometry to predict the fracture type. However, inclusion of non-uniform material properties might have refined the models, and consequently led to better discrimination accuracy, especially in the cases of trochanteric fractures which are primarily determined by BMD (Pulkkinen *et al.* 2004, Schott *et al.* 1998, 2005). This lack of accuracy was filled in study IV by using heterogeneous material properties along the PCS and PTS and in the different areas of the bone.

Whereas the methodologies used in study II and study III involved semi-automatic segmentation and eventually higher accuracy in the geometrical reconstruction of the model, the models of study IV were automatically generated from geometrical parameters for simplification of the process and high inter-user reproducibility. Furthermore, the number of bones used for the training material for this last study was quite restricted, and the accuracy of the generated shape was limited in some areas, especially on top of the trochanteric area and near the minor trochanter. Nevertheless, these areas are not crucial, since clinical hip fractures typically occur in the femoral neck and intertrochanteric regions. However, the script lacked robustness to generate bones with peculiar geometry.

The finite element methodologies in these studies were developed in order to mimic the experiment. The soft tissues, simulated by a tennis ball and a pad during the protocol, had much higher Young's modulus values than the biological tissues they were representing. As a result, overestimation of material properties

of the cartilage and other soft tissues might affect the results that could be obtained in real conditions. The potential of soft tissues to undergo big deformations and their capability to absorb energy during a fall reduces the strain transmitted to the bone. Furthermore, the cortical bone was adjusted to have a minimum thickness of 1 mm, whereas more accurate cortical values thickness might be obtained by increasing the number of elements in the models. Patient-specific evaluation of fracture risk should take into account these facts during modelling. The anisotropy of the trabecular bone could also be reflected with better accuracy using orthotropic material properties along the principal trabecular tensile and compressive systems.

6.3 Assessment of fracture type and load (II-IV)

The finite element methods used in this study seem to have the potential to discriminate the fracture type and predict experimental fracture load. The study suggests in accordance with previous studies that geometry is the most relevant factor in the discrimination of fracture type (Duboeuf *et al.* 1997, Fox *et al.* 2000, Partanen *et al.* 2001, Gnudi *et al.*2002, Szulc *et al.* 2006).

Previous studies have also reported the potential of finite elements analysis to discriminate fracture types (Keyak *et al.* 2001, Bessho *et al.* 2004, Gomez-Benito *et al.* 2005, Schileo *et al.* 2008). In general, our estimation of fracture type appeared to be more accurate than in previous studies, even if they used heterogeneous material properties. This difference in results may partly be due to the different failure criterion between studies. In their clinical study, Bessho *et al.* (2004) predicted fracture type from a crack in the cortical bone, while Keyak *et al.* (2001) used non-surface elements with the lowest factors of safety to predict the experimental fracture site. Gomez-Benito *et al.* (2005) simulated fracture type using anisotropic fracture criterion and the coefficient of risk to fracture. In our studies II and III, fracture type was estimated from the stress and strain in the trabecular bone, which appears to be an effective method in discriminating experimental hip fracture types.

We report here in study I that the tendency for a specific fracture type can already be assessed from geometrical parameters in elderly females. The results from studies II and III show an increase in the accuracy for the prediction of fracture type while compared to geometrical parameters only (Fig. 11); this suggests that FE analysis yields a more comprehensive prediction by capturing the varying stress and strain distribution caused by the shape of bone, whereas the

measurement of a limited set of local geometrical parameters provides a rougher estimate for the shape.

Previously it has been shown that trochanteric fractures are best predicted by BMD (Partanen *et al.* 2001, Eckstein *et al.* 2004, Schott *et al.* 2005, Pulkkinen *et al.* 2010). In studies II and III, both 2D and 3D geometry-based models showed lower accuracy in the prediction of this fracture type. A slight increase in the prediction accuracy between models with one and four material properties for the trabecular bone (study II) might be explained by an ambiguous stress distribution in the original model with one material property. For a femur with an individual anatomy with quite equal susceptibility for cervical and trochanteric fractures, the trabecular fine structure might define the final fracture type. In study IV, the prediction of the fracture type was based on the location of the failing of a surface element of the cortical bone (Bessho *et al.* 2007). Even if the method seems to have potential to predict fracture type, the sample size is too restricted to statistically confirm this.

As demonstrated in studies II and III, the geometry of the hip of elderly females seems to have a higher impact in the distribution of fracture types. However, for some bones with a shape without tendency for any specific fracture type, material properties might help in the discrimination of fracture type. However, study I indicates that in males, fracture type might be less related to the geometry itself than to bone mineral density. These considerations were taken into account while developing study IV, to be a compromise between geometrical accuracy and a better approximation of the non-uniformity of the bone. The neck-shaft angle being the most important geometrical parameter for fracture type prediction, it was well represented in study IV, and the orientations of the PCS and PTS were derived from it.

Multiple studies have been conducted to estimate the failure load using 3D models derived from CT scans (Keyak *et al.* 2000, 2001, Bessho *et al.* 2004, 2007, Schileo *et al.* 2007, 2008, Bessho *et al.* 2009) with high accuracy. Unfortunately, building patient-specific 3D finite element models requires high-cost volumetric imaging such as computed tomography (CT) scans involving high radiation doses and computational power. In study IV, we constructed patient-specific 3D shape with feasible accuracy, implemented with personalized material properties derived from structural analysis of the trabecular bone. The assessment of the failure load was performed from the failing of a surface element of the cortical bone (Bessho *et al.* 2007).

The predicted failure load of cervical fractures seemed to correlate better with the experimental fracture load than the predicted failure load of trochanteric fractures. As suggested previously, this might be explained by the fact that the geometry is an important factor especially for the risk of cervical fracture (Pulkkinen *et al.* 2008).

The distribution of Young's modulus in the trabecular bone was estimated based on trabecular structure analysis of the radiographs; however, the Young's modulus of the cortical bone was fixed and was similar for all the bones. Even though the trabecular bone plays a role in the strength of the upper femur (Manske *et al.* 2009), it has been demonstrated that its impact is relatively limited (Holzer *et al.* 2009). Eventually, the density of the cortical bone will not be reflected in our radiograph-based models, which results in underestimation of Young's modulus and failure load for a bone with high cortical density of the cortex. This was also confirmed in our model after verification of density from the CT scans. In future, the estimation of material properties for cortical bone might be assessed with a non-invasive ultrasound method (Nicholson, 2008).

However, preliminary results of failure load prediction were presented in study IV, and more bones will be studied in the future to reach a statistically relevant study sample size. Furthermore, the method will be developed to increase its accuracy to predict individual failure load. A feasible solution to improve the method and eventually make it applicable for clinical practice would be to use a patient-specific thickness of the soft tissues with realistic approximated material properties. The thickness could be assessed directly from medical imaging and would help in the simulation of the diffusion of load through the hip during a fall. Using this method, a study involving patients with and without hip fracture should be performed in order to evaluate if the models are able to discriminate the patients at risk.

7 Conclusions

The present study confirms that finite element models derived from radiographs can be used for preliminary assessment of fracture risk. The study suggests that fracture type can already be estimated from geometry-based finite element models whereas assessment of failure load requires patient-specific material properties. Finally, both volumetric geometry and distribution of material properties within a patient-specific model can be estimated with feasible accuracy using the analysis of a standard 2D radiograph. Based on the aims of this study, it can be specifically concluded that:

1. Intra-subject structural asymmetries are associated with different fracture types between contralateral hips of a single individual. Also, subjects with asymmetrical fracture types have different hip structures, and in males, a different hip BMD than subjects with symmetrical fracture type.
2. Experimental fracture type of females can be predicted with good accuracy from 2D finite element models derived from standard radiograph.
3. Geometry-based volumetric finite element models generated from computed tomography scans show a strain distribution associated with a specific fracture type during an experimental fall.
4. A patient-specific volumetric finite element model can be generated automatically based on a standard 2D radiograph. Such a model can estimate the failure load of an experimental simulation with feasible accuracy.

References

Ahmad O, Ramamurthi K, Wilson KE, Engelke K, Prince RL & Taylor RH (2010) Volumetric DXA (VXA): A new method to extract 3D information from multiple in vivo DXA images. J Bone Miner Res 25(12): 2744–2751.

Alegre-Lopez J, Cordero-Guevara J, Alonso-Valdivielso JL & Fernandez-Melon J (2005) Factors associated with mortality and functional disability after hip fracture: an inception cohort study. Osteoporos Int 16(7): 729–736.

Auerbach BM & Ruff CB (2006) Limb bone bilateral asymmetry: variability and commonality among modern humans. J Hum Evol 50(2): 203–218.

Baker-LePain JC, Luker KR, Lynch JA, Parimi N, Nevitt MC & Lane NE (2011) Active shape modeling of the hip in the prediction of incident hip fracture. J Bone Miner Res 26(3): 468–474.

Barry DW & Kohrt WM (2008) Exercise and the preservation of bone health. J Cardiopulm Rehabil Prev 28(3): 153–162.

Baudoin C, Fardellone P & Sebert JL (1993) Effect of sex and age on the ratio of cervical to trochanteric hip fracture. A meta-analysis of 16 reports on 36,451 cases. Acta Orthop Scand 64(6): 647–653.

Baum T, Carballido-Gamio J, Huber MB, Muller D, Monetti R, Rath C, Eckstein F, Lochmuller EM, Majumdar S, Rummeny EJ, Link TM & Bauer JS (2010) Automated 3D trabecular bone structure analysis of the proximal femur--prediction of biomechanical strength by CT and DXA. Osteoporos Int 21(9): 1553–1564.

Bayraktar HH, Morgan EF, Niebur GL, Morris GE, Wong EK & Keaveny TM (2004) Comparison of the elastic and yield properties of human femoral trabecular and cortical bone tissue. J Biomech 37(1): 27–35.

Beck TJ, Ruff CB, Warden KE, Scott WW,Jr & Rao GU (1990) Predicting femoral neck strength from bone mineral data. A structural approach. Invest Radiol 25(1): 6–18.

Beck TJ, Looker AC, Ruff CB, Sievanen H & Wahner HW (2000) Structural trends in the aging femoral neck and proximal shaft: analysis of the Third National Health and Nutrition Examination Survey dual-energy X-ray absorptiometry data. J Bone Miner Res 15(12): 2297–2304.

Beck TJ, Oreskovic TL, Stone KL, Ruff CB, Ensrud K, Nevitt MC, Genant HK & Cummings SR (2001) Structural adaptation to changing skeletal load in the progression toward hip fragility: the study of osteoporotic fractures. J Bone Miner Res 16(6): 1108–1119.

Benhamou CL, Poupon S, Lespessailles E, Loiseau S, Jennane R, Siroux V, Ohley W & Pothuaud L (2001) Fractal analysis of radiographic trabecular bone texture and bone mineral density: two complementary parameters related to osteoporotic fractures. J Bone Miner Res 16(4): 697–704.

Bentler SE, Liu L, Obrizan M, Cook EA, Wright KB, Geweke JF, Chrischilles EA, Pavlik CE, Wallace RB, Ohsfeldt RL, Jones MP, Rosenthal GE & Wolinsky FD (2009) The aftermath of hip fracture: discharge placement, functional status change, and mortality. Am J Epidemiol 170(10): 1290–1299.

Bergot C, Bousson V, Meunier A, Laval-Jeantet M & Laredo JD (2002) Hip fracture risk and proximal femur geometry from DXA scans. Osteoporos Int 13(7): 542–550.

Bessho M, Ohnishi I, Okazaki H, Sato W, Kominami H, Matsunaga S & Nakamura K (2004) Prediction of the strength and fracture location of the femoral neck by CT-based finite-element method: a preliminary study on patients with hip fracture. J Orthop Sci 9(6): 545–550.

Bessho M, Ohnishi I, Matsuyama J, Matsumoto T, Imai K & Nakamura K (2007) Prediction of strength and strain of the proximal femur by a CT-based finite element method. J Biomech 40(8): 1745–1753.

Bessho M, Ohnishi I, Matsumoto T, Ohashi S, Matsuyama J, Tobita K, Kaneko M & Nakamura K (2009) Prediction of proximal femur strength using a CT-based nonlinear finite element method: differences in predicted fracture load and site with changing load and boundary conditions. Bone 45(2): 226–231.

Bonewald LF (2011). The amazing osteocyte. J Bone Miner Res. 26(2):229–38.

Bousson V, Le Bras A, Roqueplan F, Kang Y, Mitton D, Kolta S, Bergot C, Skalli W, Vicaut E, Kalender W, Engelke K & Laredo JD (2006) Volumetric quantitative computed tomography of the proximal femur: relationships linking geometric and densitometric variables to bone strength. Role for compact bone. Osteoporos Int 17(6): 855–864.

Bousson V, Wybier M, Petrover D, Parlier C, Chicheportiche V, Hamze B, Sverzut JM, Daguet E, Wyler A, Thabet J, Bossard P & Laredo JD (2011) Stress fractures. J Radiol 92(3): 188–207.

Boyce WJ & Vessey MP (1985) Rising incidence of fracture of the proximal femur. Lancet 1(8421): 150–151.

Briot B (1980) Fractures per-trochantériennes: anatomie pathologique et classification. Cahiers d'Enseignement de la SOFCOT Expansions Sci Franc 12: 69–76.

Brownbill RA, Lindsey C, Crncevic-Orlic Z & Ilich JZ (2003) Dual hip bone mineral density in postmenopausal women: geometry and effect of physical activity. Calcif Tissue Int 73(3): 217–224.

Bryan R, Nair PB & Taylor M (2009) Use of a statistical model of the whole femur in a large scale, multi-model study of femoral neck fracture risk. J Biomech 42(13): 2171–2176.

Bryan R, Mohan PS, Hopkins A, Galloway F, Taylor M & Nair PB (2010) Statistical modelling of the whole human femur incorporating geometric and material properties. Med Eng Phys 32(1): 57–65.

Burr DB (2002a) Bone material properties and mineral matrix contributions to fracture risk or age in women and men. J Musculoskelet Neuronal Interact 2(3): 201–204.

Burr DB (2002b) The contribution of the organic matrix to bone's material properties. Bone 31(1): 8–11.

Carter DR & Hayes WC (1977) The compressive behavior of bone as a two-phase porous structure. J Bone Joint Surg Am 59(7): 954–962.

Cauley JA, Lui LY, Genant HK, Salamone L, Browner W, Fink HA, Cohen P, Hillier T, Bauer DC, Cummings SR & Study of Osteoporotic Fractures Research and Group (2009) Risk factors for severity and type of the hip fracture. J Bone Miner Res 24(5): 943–955.

Chappard D, Chennebault A, Moreau M, Legrand E, Audran M & Basle MF (2001) Texture analysis of X-ray radiographs is a more reliable descriptor of bone loss than mineral content in a rat model of localized disuse induced by the Clostridium botulinum toxin. Bone 28(1): 72–79.

Chappard D, Guggenbuhl P, Legrand E, Basle MF & Audran M (2005) Texture analysis of X-ray radiographs is correlated with bone histomorphometry. J Bone Miner Metab 23(1): 24–29.

Chappard C, Bousson V, Bergot C, Mitton D, Marchadier A, Moser T, Benhamou CL & Laredo JD (2010) Prediction of femoral fracture load: cross-sectional study of texture analysis and geometric measurements on plain radiographs versus bone mineral density. Radiology 255(2): 536–543.

Cheng H, Gary LC, Curtis JR, Saag KG, Kilgore ML, Morrisey MA, Matthews R, Smith W, Yun H & Delzell E (2009) Estimated prevalence and patterns of presumed osteoporosis among older Americans based on Medicare data. Osteoporos Int 20(9): 1507–1515.

Cheng X, Li J, Lu Y, Keyak J & Lang T (2007) Proximal femoral density and geometry measurements by quantitative computed tomography: association with hip fracture. Bone 40(1): 169–174.

Cody DD, Gross GJ, Hou FJ, Spencer HJ, Goldstein SA & Fyhrie DP (1999) Femoral strength is better predicted by finite element models than QCT and DXA. J Biomech 32(10): 1013–1020.

Cody DD, Divine GW, Nahigian K & Kleerekoper M (2000a) Bone density distribution and gender dominate femoral neck fracture risk predictors. Skeletal Radiol 29(3): 151–161.

Cody DD, Hou FJ, Divine GW & Fyhrie DP (2000b) Femoral structure and stiffness in patients with femoral neck fracture. J Orthop Res 18(3): 443–448.

Cornwall R, Gilbert MS, Koval KJ, Strauss E & Siu AL (2004) Functional outcomes and mortality vary among different types of hip fractures: a function of patient characteristics. Clin Orthop Relat Res (425)(425): 64–71.

Courtney AC, Wachtel EF, Myers ER & Hayes WC (1994) Effects of loading rate on strength of the proximal femur. Calcif Tissue Int 55(1): 53–58.

Courtney AC, Wachtel EF, Myers ER & Hayes WC (1995) Age-related reductions in the strength of the femur tested in a fall-loading configuration. J Bone Joint Surg Am 77(3): 387–395.

Crabtree N, Lunt M, Holt G, Kroger H, Burger H, Grazio S, Khaw KT, Lorenc RS, Nijs J, Stepan J, Falch JA, Miazgowski T, Raptou P, Pols HA, Dequeker J, Havelka S, Hoszowski K, Jajic I, Czekalski S, Lyritis G, Silman AJ & Reeve J (2000) Hip geometry, bone mineral distribution, and bone strength in European men and women: the EPOS study. Bone 27(1): 151–159.

Crabtree NJ, Kroger H, Martin A, Pols HA, Lorenc R, Nijs J, Stepan JJ, Falch JA, Miazgowski T, Grazio S, Raptou P, Adams J, Collings A, Khaw KT, Rushton N, Lunt M, Dixon AK & Reeve J (2002) Improving risk assessment: hip geometry, bone mineral distribution and bone strength in hip fracture cases and controls. The EPOS study. European Prospective Osteoporosis Study. Osteoporos Int 13(1): 48–54.

Crawford RP, Cann CE & Keaveny TM (2003) Finite element models predict in vitro vertebral body compressive strength better than quantitative computed tomography. Bone 33(4): 744–750.

Cuk T, Leben-Seljak P & Stefancic M (2001) Lateral asymmetry of human long bones. Variabil Evolut 9: 19–32.

Cummings SR (1985) Are patients with hip fractures more osteoporotic? Review of the evidence. Am J Med 78(3): 487–494.

Cummings SR, Nevitt MC, Browner WS, Stone K, Fox KM, Ensrud KE, Cauley J, Black D & Vogt TM (1995) Risk factors for hip fracture in white women. Study of Osteoporotic Fractures Research Group. N Engl J Med 332(12): 767–773.

Cummings SR & Melton LJ (2002) Epidemiology and outcomes of osteoporotic fractures. Lancet 359(9319): 1761–1767.

Currey JD (2001) Bone strength: what are we trying to measure? Calcif Tissue Int 68(4): 205–210.

Currey JD (2003a) How well are bones designed to resist fracture? J Bone Miner Res 18(4): 591–598.

Currey JD (2003b) The many adaptations of bone. J Biomech 36(10): 1487–1495.

Da Costa JA, Ribeiro A, Bogas M, Costa L, Varino C, Lucas R, Rodrigues A & Araujo D (2009) Mortality and functional impairment after hip fracture - a prospective study in a Portuguese population. Acta Reumatol Port 34(4): 618–626.

Drucker DC and Prager W (1952) Soil mechanics and plastic analysis for limit design. Quart Appl Math 10:157–165.

Duan Y, Beck TJ, Wang XF & Seeman E (2003) Structural and biomechanical basis of sexual dimorphism in femoral neck fragility has its origins in growth and aging. J Bone Miner Res 18(10): 1766–1774.

Duboeuf F, Hans D, Schott AM, Kotzki PO, Favier F, Marcelli C, Meunier PJ & Delmas PD (1997) Different morphometric and densitometric parameters predict cervical and trochanteric hip fracture: the EPIDOS Study. J Bone Miner Res 12(11): 1895–1902.

Duchemin L, Mitton D, Jolivet E, Bousson V, Laredo JD & Skalli W (2008a) An anatomical subject-specific FE-model for hip fracture load prediction. Comput Methods Biomech Biomed Engin 11(2): 105–111.

Duchemin L, Bousson V, Raossanaly C, Bergot C, Laredo JD, Skalli W & Mitton D (2008b) Prediction of mechanical properties of cortical bone by quantitative computed tomography. Med Eng Phys 30(3): 321–328.

Dwek JR (2010) The periosteum: what is it, where is it, and what mimics it in its absence? Skeletal Radiol 39(4): 319–323.

Eckstein F, Lochmuller EM, Lill CA, Kuhn V, Schneider E, Delling G & Muller R (2002) Bone strength at clinically relevant sites displays substantial heterogeneity and is best predicted from site-specific bone densitometry. J Bone Miner Res 17(1): 162–171.

Eckstein F, Wunderer C, Boehm H, Kuhn V, Priemel M, Link TM & Lochmuller EM (2004) Reproducibility and side differences of mechanical tests for determining the structural strength of the proximal femur. J Bone Miner Res 19(3): 379–385.

Eriksen EF (2010). Cellular mechanisms of bone remodeling. Rev Endocr Metab Disord. 11(4):219–27.

Evans E (1949) The treatment of trochanteric fractures of the femur. J Bone Joint Surg 31 B: 190–203.

Farmer ME, White LR, Brody JA & Bailey KR (1984) Race and sex differences in hip fracture incidence. Am J Public Health 74(12): 1374–1380.

Faulkner KG, Genant HK & McClung M (1995) Bilateral comparison of femoral bone density and hip axis length from single and fan beam DXA scans. Calcif Tissue Int 56(1): 26–31.

Fox KM, Cummings SR, Williams E, Stone K & Study of Osteoporotic Fractures (2000) Femoral neck and intertrochanteric fractures have different risk factors: a prospective study. Osteoporos Int 11(12): 1018–1023.

Frost HM (1994) Wolff's Law and bone's structural adaptations to mechanical usage: an overview for clinicians. Angle Orthod 64(3): 175–188.

Frost HM (2004) A 2003 update of bone physiology and Wolff's Law for clinicians. Angle Orthod 74(1): 3–15.

Galibarov PE, Prendergast PJ & Lennon AB (2010) A method to reconstruct patient-specific proximal femur surface models from planar pre-operative radiographs. Med Eng Phys 32(10): 1180–1188.

Garden RS Low-angle fixation in fractures of the femoral neck. Journal of Bone and Joint Surgery 43b: 647–663.

Geusens P, Autier P, Boonen S, Vanhoof J, Declerck K & Raus J (2002) The relationship among history of falls, osteoporosis, and fractures in postmenopausal women. Arch Phys Med Rehabil 83(7): 903–906.

Gillespie LD, Robertson MC, Gillespie WJ, Lamb SE, Gates S, Cumming RG & Rowe BH (2009) Interventions for preventing falls in older people living in the community. Cochrane Database Syst Rev (2)(2): CD007146.

Gnudi S, Ripamonti C, Lisi L, Fini M, Giardino R & Giavaresi G (2002) Proximal femur geometry to detect and distinguish femoral neck fractures from trochanteric fractures in postmenopausal women. Osteoporos Int 13(1): 69–73.

Gomez-Benito MJ, Garcia-Aznar JM & Doblare M (2005) Finite element prediction of proximal femoral fracture patterns under different loads. J Biomech Eng 127(1): 9–14.

Gregg EW, Pereira MA & Caspersen CJ (2000) Physical activity, falls, and fractures among older adults: a review of the epidemiologic evidence. J Am Geriatr Soc 48(8): 883–893.

Gregory JS, Stewart A, Undrill PE, Reid DM & Aspden RM (2004a) Identification of hip fracture patients from radiographs using Fourier analysis of the trabecular structure: a cross-sectional study. BMC Med Imaging 4(1): 4.

Gregory JS, Testi D, Stewart A, Undrill PE, Reid DM & Aspden RM (2004b) A method for assessment of the shape of the proximal femur and its relationship to osteoporotic hip fracture. Osteoporos Int 15(1): 5–11.

Gregory JS, Stewart A, Undrill PE, Reid DM & Aspden RM (2005) Bone shape, structure, and density as determinants of osteoporotic hip fracture: a pilot study investigating the combination of risk factors. Invest Radiol 40(9): 591–597.

Gregory JS, Waarsing JH, Day J, Pols HA, Reijman M, Weinans H & Aspden RM (2007) Early identification of radiographic osteoarthritis of the hip using an active shape model to quantify changes in bone morphometric features: can hip shape tell us anything about the progression of osteoarthritis? Arthritis Rheum 56(11): 3634–3643.

Gregory JS & Aspden RM (2008) Femoral geometry as a risk factor for osteoporotic hip fracture in men and women. Med Eng Phys 30(10): 1275–1286.

Grisso JA, Kelsey JL, Strom BL, Chiu GY, Maislin G, O'Brien LA, Hoffman S & Kaplan F (1991a) Risk factors for falls as a cause of hip fracture in women. The Northeast Hip Fracture Study Group. N Engl J Med 324(19): 1326–1331.

Grisso JA, Chiu GY, Maislin G, Steinmann WC & Portale J (1991b) Risk factors for hip fractures in men: a preliminary study. J Bone Miner Res 6(8): 865–868.

Groen BE, Smulders E, de Kam D, Duysens J & Weerdesteyn V (2010) Martial arts fall training to prevent hip fractures in the elderly. Osteoporos Int 21(2): 215–221.

Gullberg B, Johnell O & Kanis JA (1997) World-wide projections for hip fracture. Osteoporos Int 7(5): 407–413.

Gunay M, Shim MB & Shimada K (2007) Cost- and time-effective three-dimensional bone-shape reconstruction from X-ray images. Int J Med Robot 3(4): 323–335.

Haapasalo H, Kannus P, Sievanen H, Pasanen M, Uusi-Rasi K, Heinonen A, Oja P & Vuori I (1996) Development of mass, density, and estimated mechanical characteristics of bones in Caucasian females. J Bone Miner Res 11(11): 1751–1760.

Haentjens P, Autier P, Barette M, Venken K, Vanderschueren D, Boonen S & Hip Fracture Study Group (2007) Survival and functional outcome according to hip fracture type: a one-year prospective cohort study in elderly women with an intertrochanteric or femoral neck fracture. Bone 41(6): 958–964.

Hans D, Genton L, Drezner MK, Schott AM, Pacifici R, Avioli L, Slosman DO & Meunier PJ (2002) Monitored impact loading of the hip: initial testing of a home-use device. Calcif Tissue Int 71(2): 112–120.

Heaney RP, Barger-Lux MJ, Davies KM, Ryan RA, Johnson ML & Gong G (1997) Bone dimensional change with age: interactions of genetic, hormonal, and body size variables. Osteoporos Int 7(5): 426–431.

Hochberg MC, Williamson J, Skinner EA, Guralnik J, Kasper JD & Fried LP (1998) The prevalence and impact of self-reported hip fracture in elderly community-dwelling women: the Women's Health and Aging Study. Osteoporos Int 8(4): 385–389.

Holzer G, von Skrbensky G, Holzer LA & Pichl W (2009) Hip fractures and the contribution of cortical versus trabecular bone to femoral neck strength. J Bone Miner Res 24(3): 468–474.

Huber MB, Carballido-Gamio J, Bauer JS, Baum T, Eckstein F, Lochmuller EM, Majumdar S & Link TM (2008) Proximal femur specimens: automated 3D trabecular bone mineral density analysis at multidetector CT--correlation with biomechanical strength measurement. Radiology 247(2): 472–481.

Huber MB, Carballido-Gamio J, Fritscher K, Schubert R, Haenni M, Hengg C, Majumdar S & Link TM (2009) Development and testing of texture discriminators for the analysis of trabecular bone in proximal femur radiographs. Med Phys 36(11): 5089–5098.

Isaac B, Vettivel S, Prasad R, Jeyaseelan L & Chandi G (1997) Prediction of the femoral neck-shaft angle from the length of the femoral neck. Clin Anat 10(5): 318–323.

Ito M, Wakao N, Hida T, Matsui Y, Abe Y, Aoyagi K, Uetani M & Harada A (2010) Analysis of hip geometry by clinical CT for the assessment of hip fracture risk in elderly Japanese women. Bone 46(2): 453–457.

Jamsa T, Vainionpaa A, Korpelainen R, Vihriala E & Leppaluoto J (2006) Effect of daily physical activity on proximal femur. Clin Biomech (Bristol, Avon) 21(1): 1–7.

Johnell O, Kanis JA, Oden A, Sernbo I, Redlund-Johnell I, Petterson C, De Laet C & Jonsson B (2004) Mortality after osteoporotic fractures. Osteoporos Int 15(1): 38–42.

Jokinen H, Pulkkinen P, Korpelainen J, Heikkinen J, Keinanen-Kiukaanniemi S, Jamsa T & Korpelainen R (2010) Risk factors for cervical and trochanteric hip fractures in elderly women: a population-based 10-year follow-up study. Calcif Tissue Int 87(1): 44–51.

Kam D, Smulders E, Weerdesteyn V & Smits-Engelsman BC (2009) Exercise interventions to reduce fall-related fractures and their risk factors in individuals with low bone density: a systematic review of randomized controlled trials. Osteoporos Int 20(12): 2111–2125.

Kanchan T, Mohan Kumar TS, Pradeep Kumar G & Yoganarasimha K (2008) Skeletal asymmetry. J Forensic Leg Med 15(3): 177–179.

Kanis JA (1994) Assessment of fracture risk and its application to screening for postmenopausal osteoporosis: synopsis of a WHO report. WHO Study Group. Osteoporos Int 4(6): 368–381.

Kanis JA, Johnell O, Oden A, Dawson A, De Laet C & Jonsson B (2001) Ten year probabilities of osteoporotic fractures according to BMD and diagnostic thresholds. Osteoporos Int 12(12): 989–995.

Kanis JA (2002) Diagnosis of osteoporosis and assessment of fracture risk. Lancet 359(9321): 1929–1936.

Kanis JA, Borgstrom F, De Laet C, Johansson H, Johnell O, Jonsson B, Oden A, Zethraeus N, Pfleger B & Khaltaev N (2005) Assessment of fracture risk. Osteoporos Int 16(6): 581–589.

Kanis JA, McCloskey EV, Johansson H, Oden A, Melton LJ,3rd & Khaltaev N (2008a) A reference standard for the description of osteoporosis. Bone 42(3): 467–475.

Kanis JA, Johnell O, Oden A, Johansson H & McCloskey E (2008b) FRAX and the assessment of fracture probability in men and women from the UK. Osteoporos Int 19(4): 385–397.

Kannus P, Parkkari J, Sievanen H, Heinonen A, Vuori I & Jarvinen M (1996) Epidemiology of hip fractures. Bone 18(1 Suppl): 57S–63S.

Kannus P, Niemi S, Parkkari J, Palvanen M, Vuori I & Jarvinen M (1999) Hip fractures in Finland between 1970 and 1997 and predictions for the future. Lancet 353(9155): 802–805.

Kannus P, Niemi S, Parkkari J, Palvanen M, Vuori I & Jarvinen M (2006) Nationwide decline in incidence of hip fracture. J Bone Miner Res 21(12): 1836–1838.

Kaptoge S, Dalzell N, Loveridge N, Beck TJ, Khaw KT & Reeve J (2003) Effects of gender, anthropometric variables, and aging on the evolution of hip strength in men and women aged over 65. Bone 32(5): 561–570.

Kaptoge S, Benevolenskaya LI, Bhalla AK, Cannata JB, Boonen S, Falch JA, Felsenberg D, Finn JD, Nuti R, Hoszowski K, Lorenc R, Miazgowski T, Jajic I, Lyritis G, Masaryk P, Naves-Diaz M, Poor G, Reid DM, Scheidt-Nave C, Stepan JJ, Todd CJ, Weber K, Woolf AD, Roy DK, Lunt M, Pye SR, O'neill TW, Silman AJ & Reeve J (2005) Low BMD is less predictive than reported falls for future limb fractures in women across Europe: results from the European Prospective Osteoporosis Study. Bone 36(3): 387–398.

Keene GS, Parker MJ & Pryor GA (1993) Mortality and morbidity after hip fractures. BMJ 307(6914): 1248–1250.

Keller TS (1994) Predicting the compressive mechanical behavior of bone. J Biomech 27(9): 1159–1168.

Keyak JH, Lee IY & Skinner HB (1994) Correlations between orthogonal mechanical properties and density of trabecular bone: use of different densitometric measures. J Biomed Mater Res 28(11): 1329–1336.

Keyak JH, Rossi SA, Jones KA & Skinner HB (1998) Prediction of femoral fracture load using automated finite element modeling. J Biomech 31(2): 125–133.

Keyak JH, Rossi SA, Jones KA, Les CM & Skinner HB (2001) Prediction of fracture location in the proximal femur using finite element models. Med Eng Phys 23(9): 657–664.

Keyak JH & Falkinstein Y (2003) Comparison of in situ and in vitro CT scan-based finite element model predictions of proximal femoral fracture load. Med Eng Phys 25(9): 781–787.

Lang TF, Keyak JH, Heitz MW, Augat P, Lu Y, Mathur A & Genant HK (1997) Volumetric quantitative computed tomography of the proximal femur: precision and relation to bone strength. Bone 21(1): 101–108.

Langton CM, Pisharody S & Keyak JH (2009a) Comparison of 3D finite element analysis derived stiffness and BMD to determine the failure load of the excised proximal femur. Med Eng Phys 31(6): 668–672.

Langton CM, Pisharody S & Keyak JH (2009b) Generation of a 3D proximal femur shape from a single projection 2D radiographic image. Osteoporos Int 20(3): 455–461.

Lengsfeld M, Schmitt J, Alter P, Kaminsky J & Leppek R (1998) Comparison of geometry-based and CT voxel-based finite element modelling and experimental validation. Med Eng Phys 20(7): 515–522.

Lochmuller EM, Groll O, Kuhn V & Eckstein F (2002) Mechanical strength of the proximal femur as predicted from geometric and densitometric bone properties at the lower limb versus the distal radius. Bone 30(1): 207–216.

Lochmuller EM, Muller R, Kuhn V, Lill CA & Eckstein F (2003) Can novel clinical densitometric techniques replace or improve DXA in predicting bone strength in osteoporosis at the hip and other skeletal sites? J Bone Miner Res 18(5): 906–912.

Lotz JC, Cheal EJ & Hayes WC (1991a) Fracture prediction for the proximal femur using finite element models: Part I--Linear analysis. J Biomech Eng 113(4): 353–360.

Lotz JC, Cheal EJ & Hayes WC (1991b) Fracture prediction for the proximal femur using finite element models: Part II--Nonlinear analysis. J Biomech Eng 113(4): 361–365.

Luthje P, Nurmi-Luthje I, Kaukonen JP, Kuurne S, Naboulsi H & Kataja M (2009) Undertreatment of osteoporosis following hip fracture in the elderly. Arch Gerontol Geriatr 49(1): 153–157.

Mabesoone F (1997). Maitrise orthopédique 65

Macho GA (1991) Anthropological evaluation of left-right differences in the femur of southern African populations. Anthropol Anz 49(3): 207–216.

Majumder S, Roychowdhury A & Pal S (2007) Simulation of hip fracture in sideways fall using a 3D finite element model of pelvis-femur-soft tissue complex with simplified representation of whole body. Med Eng Phys 29(10): 1167–1178.

Manske SL, Liu-Ambrose T, Cooper DM, Kontulainen S, Guy P, Forster BB & McKay HA (2009) Cortical and trabecular bone in the femoral neck both contribute to proximal femur failure load prediction. Osteoporos Int 20(3): 445–453.

Marks R, Allegrante JP, Ronald MacKenzie C & Lane JM (2003) Hip fractures among the elderly: causes, consequences and control. Ageing Res Rev 2(1): 57–93.

Marshall D, Johnell O & Wedel H (1996) Meta-analysis of how well measures of bone mineral density predict occurrence of osteoporotic fractures. BMJ 312(7041): 1254–1259.

Martens M, Van Audekercke R, Delport P, De Meester P & Mulier JC (1983) The mechanical characteristics of cancellous bone at the upper femoral region. J Biomech 16(12): 971–983.

Mautalen CA, Vega EM & Einhorn TA (1996) Are the etiologies of cervical and trochanteric hip fractures different? Bone 18(3 Suppl): 133S–137S.

Mayhew PM, Thomas CD, Clement JG, Loveridge N, Beck TJ, Bonfield W, Burgoyne CJ & Reeve J (2005) Relation between age, femoral neck cortical stability, and hip fracture risk. Lancet 366(9480): 129–135.

Melton LJ,3rd (1996) Epidemiology of hip fractures: implications of the exponential increase with age. Bone 18(3 Suppl): 121S–125S.

Meta M, Lu Y, Keyak JH & Lang T (2006) Young-elderly differences in bone density, geometry and strength indices depend on proximal femur sub-region: a cross sectional study in Caucasian-American women. Bone 39(1): 152–158.

Meyer HE, Tverdal A, Falch JA & Pedersen JI (2000) Factors associated with mortality after hip fracture. Osteoporos Int 11(3): 228–232.

Michelotti J & Clark J (1999) Femoral neck length and hip fracture risk. J Bone Miner Res 14(10): 1714–1720.

Morgan EF & Keaveny TM (2001) Dependence of yield strain of human trabecular bone on anatomic site. J Biomech 34(5): 569–577.

Morgan EF, Bayraktar HH & Keaveny TM (2003) Trabecular bone modulus-density relationships depend on anatomic site. J Biomech 36(7): 897–904.

Morita S, Jinno T, Nakamura H, Kumei Y, Shinomiya K & Yamamoto H (2005) Bone mineral density and walking ability of elderly patients with hip fracture: a strategy for prevention of hip fracture. Injury 36(9): 1075–1079.

Muller ME (1980) Classification and international AO-documentation of femur fractures. Unfallheilkunde 83(5): 251–259.

Muller ME & Nazarian S (1981) Classification of fractures of the femur and its use in the A.O. index (author's transl). Rev Chir Orthop Reparatrice Appar Mot 67(3): 297–309.

Neve A, Corrado A, Cantatore FP (2011). Osteoblast physiology in normal and pathological conditions. Cell Tissue Res. 343(2):289–302.

Nicholson PHF (2008). Ultrasound and the Biomechanical Competence of Bone. IEEE Trans Ultrason Ferroelectr Freq Control., 55 (7): 1539–1545.

Ota T, Yamamoto I & Morita R (1999) Fracture simulation of the femoral bone using the finite-element method: how a fracture initiates and proceeds. J Bone Miner Metab 17(2): 108–112.

Ozturk A, Ozkan Y, Akgoz S, Yalcyn N, Ozdemir RM & Aykut S (2010) The risk factors for mortality in elderly patients with hip fractures: postoperative one-year results. Singapore Med J 51(2): 137–143.

Parkkari J, Kannus P, Palvanen M, Natri A, Vainio J, Aho H, Vuori I & Jarvinen M (1999) Majority of hip fractures occur as a result of a fall and impact on the greater trochanter of the femur: a prospective controlled hip fracture study with 206 consecutive patients. Calcif Tissue Int 65(3): 183–187.

Partanen J, Jamsa T & Jalovaara P (2001) Influence of the upper femur and pelvic geometry on the risk and type of hip fractures. J Bone Miner Res 16(8): 1540–1546.

Peng L, Bai J, Zeng X & Zhou Y (2006) Comparison of isotropic and orthotropic material property assignments on femoral finite element models under two loading conditions. Med Eng Phys 28(3): 227–233.

Pinilla TP, Boardman KC, Bouxsein ML, Myers ER & Hayes WC (1996) Impact direction from a fall influences the failure load of the proximal femur as much as age-related bone loss. Calcif Tissue Int 58(4): 231–235.

Pulkkinen P, Partanen J, Jalovaara P & Jamsa T (2004) Combination of bone mineral density and upper femur geometry improves the prediction of hip fracture. Osteoporos Int 15(4): 274–280.

Pulkkinen P, Eckstein F, Lochmuller EM, Kuhn V & Jamsa T (2006) Association of geometric factors and failure load level with the distribution of cervical vs. trochanteric hip fractures. J Bone Miner Res 21(6): 895–901.

Pulkkinen P, Jamsa T, Lochmuller EM, Kuhn V, Nieminen MT & Eckstein F (2008) Experimental hip fracture load can be predicted from plain radiography by combined analysis of trabecular bone structure and bone geometry. Osteoporos Int 19(4): 547–558.

Pulkkinen P, Partanen J, Jalovaara P & Jamsa T (2010) BMD T-score discriminates trochanteric fractures from unfractured controls, whereas geometry discriminates cervical fracture cases from unfractured controls of similar BMD. Osteoporos Int 21(7): 1269–1276.

Qian JG, Song YW, Tang X & Zhang S (2009) Examination of femoral-neck structure using finite element model and bone mineral density using dual-energy X-ray absorptiometry. Clin Biomech (Bristol, Avon) 24(1): 47–52.

Ramadier JO, Duparc J, Rougemont D & De Ferrari G (1956) Surgical treatment of trochanteric and juxta-trochanteric fractures. Rev Chir Orthop Reparatrice Appar Mot 42(6): 759–82; discussion, 782–6.

Rice JC, Cowin SC & Bowman JA (1988) On the dependence of the elasticity and strength of cancellous bone on apparent density. J Biomech 21(2): 155–168.

Riggs BL, Melton Iii LJ,3rd, Robb RA, Camp JJ, Atkinson EJ, Peterson JM, Rouleau PA, McCollough CH, Bouxsein ML & Khosla S (2004) Population-based study of age and sex differences in bone volumetric density, size, geometry, and structure at different skeletal sites. J Bone Miner Res 19(12): 1945–1954.

Rivadeneira F, Zillikens MC, De Laet CE, Hofman A, Uitterlinden AG, Beck TJ & Pols HA (2007) Femoral neck BMD is a strong predictor of hip fracture susceptibility in elderly men and women because it detects cortical bone instability: the Rotterdam Study. J Bone Miner Res 22(11): 1781–1790.

Robling AG, Hinant FM, Burr DB & Turner CH (2002) Improved bone structure and strength after long-term mechanical loading is greatest if loading is separated into short bouts. J Bone Miner Res 17(8): 1545–1554.

Robling AG, Castillo AB & Turner CH (2006) Biomechanical and molecular regulation of bone remodeling. Annu Rev Biomed Eng 8: 455–498.

Roesler H (1987) The history of some fundamental concepts in bone biomechanics. J Biomech 20(11–12): 1025–1034.

Rudman KE, Aspden RM & Meakin JR (2006) Compression or tension? The stress distribution in the proximal femur. Biomed Eng Online 5: 12.

Ruff C, Holt B & Trinkaus E (2006) Who's afraid of the big bad Wolff?: "Wolff's law" and bone functional adaptation. Am J Phys Anthropol 129(4): 484–498.

Sadowsky O, Cohen JD & Taylor RH (2006) Projected tetrahedra revisited: a barycentric formulation applied to digital radiograph reconstruction using higher-order attenuation functions. IEEE Trans Vis Comput Graph 12(4): 461–473.

Sadowsky O, Chintalapani G & Taylor RH (2007) Deformable 2D-3D registration of the pelvis with a limited field of view, using shape statistics. Med Image Comput Comput Assist Interv 10(Pt 2): 519–526.

Samaha AA, Ivanov AV, Haddad JJ, Kolesnik AI, Baydoun S, Arabi MR, Yashina IN, Samaha RA & Ivanov DA (2008) Asymmetry and structural system analysis of the proximal femur meta-epiphysis: osteoarticular anatomical pathology. J Orthop Surg 3: 11.

Schileo E, Taddei F, Malandrino A, Cristofolini L & Viceconti M (2007) Subject-specific finite element models can accurately predict strain levels in long bones. J Biomech 40(13): 2982–2989.

Schileo E, Taddei F, Cristofolini L & Viceconti M (2008) Subject-specific finite element models implementing a maximum principal strain criterion are able to estimate failure risk and fracture location on human femurs tested in vitro. J Biomech 41(2): 356–367.

Schott AM, Cormier C, Hans D, Favier F, Hausherr E, Dargent-Molina P, Delmas PD, Ribot C, Sebert JL, Breart G & Meunier PJ (1998) How hip and whole-body bone mineral density predict hip fracture in elderly women: the EPIDOS Prospective Study. Osteoporos Int 8(3): 247–254.

Schott AM, Hans D, Duboeuf F, Dargent-Molina P, Hajri T, Breart G, Meunier PJ & EPIDOS Study Group (2005) Quantitative ultrasound parameters as well as bone mineral density are better predictors of trochanteric than cervical hip fractures in elderly women. Results from the EPIDOS study. Bone 37(6): 858–863.

Schuit SC, van der Klift M, Weel AE, de Laet CE, Burger H, Seeman E, Hofman A, Uitterlinden AG, van Leeuwen JP & Pols HA (2004) Fracture incidence and association with bone mineral density in elderly men and women: the Rotterdam Study. Bone 34(1): 195–202.

Schumann S, Tannast M, Nolte LP & Zheng G (2010) Validation of statistical shape model based reconstruction of the proximal femur--A morphology study. Med Eng Phys 32(6): 638–644.

Seeman E & Delmas PD (2006) Bone quality--the material and structural basis of bone strength and fragility. N Engl J Med 354(21): 2250–2261.

Seeman E (2007) The periosteum--a surface for all seasons. Osteoporos Int 18(2): 123–128.

Seeman E (2008) Bone quality: the material and structural basis of bone strength. J Bone Miner Metab 26(1): 1–8.

Sernbo I & Johnell O (1993) Consequences of a hip fracture: a prospective study over 1 year. Osteoporos Int 3(3): 148–153.

Sievanen H, Kannus P, Nieminen V, Heinonen A, Oja P & Vuori I (1996) Estimation of various mechanical characteristics of human bones using dual energy X-ray absorptiometry: methodology and precision. Bone 18(1 Suppl): 17S–27S.

Sievanen H & Kannus P (2007a) Physical activity reduces the risk of fragility fracture. PLoS Med 4(6): e222.

Sievanen H, Jozsa L, Pap I, Jarvinen M, Jarvinen TA, Kannus P & Jarvinen TL (2007b) Fragile external phenotype of modern human proximal femur in comparison with medieval bone. J Bone Miner Res 22(4): 537–543.

Singh M, Nagrath AR & Maini PS (1970) Changes in trabecular pattern of the upper end of the femur as an index of osteoporosis. J Bone Joint Surg Am 52(3): 457–467.

Stevens JA & Olson S (2000) Reducing falls and resulting hip fractures among older women. MMWR Recomm Rep 49(RR-2): 3–12.

Stone KL, Seeley DG, Lui LY, Cauley JA, Ensrud K, Browner WS, Nevitt MC, Cummings SR & Osteoporotic Fractures Research Group (2003) BMD at multiple sites and risk of fracture of multiple types: long-term results from the Study of Osteoporotic Fractures. J Bone Miner Res 18(11): 1947–1954.

Szulc P, Duboeuf F, Schott AM, Dargent-Molina P, Meunier PJ & Delmas PD (2006) Structural determinants of hip fracture in elderly women: re-analysis of the data from the EPIDOS study. Osteoporos Int 17(2): 231–236.

Taddei F, Schileo E, Helgason B, Cristofolini L & Viceconti M (2007) The material mapping strategy influences the accuracy of CT-based finite element models of bones: an evaluation against experimental measurements. Med Eng Phys 29(9): 973–979.

Testi D, Viceconti M, Baruffaldi F & Cappello A (1999) Risk of fracture in elderly patients: a new predictive index based on bone mineral density and finite element analysis. Comput Methods Programs Biomed 60(1): 23–33.

Testi D, Viceconti M, Cappello A & Gnudi S (2002) Prediction of hip fracture can be significantly improved by a single biomedical indicator. Ann Biomed Eng 30(6): 801–807.

Testi D, Cappello A, Sgallari F, Rumpf M & Viceconti M (2004) A new software for prediction of femoral neck fractures. Comput Methods Programs Biomed 75(2): 141–145.

Turner CH (1998) Three rules for bone adaptation to mechanical stimuli. Bone 23(5): 399–407.

Turner CH & Robling AG (2003) Designing exercise regimens to increase bone strength. Exerc Sport Sci Rev 31(1): 45–50.

Vaananen SP, Isaksson H, Julkunen P, Sirola J, Kroger H & Jurvelin JS (2010) Assessment of the 3-D shape and mechanics of the proximal femur using a shape template and a bone mineral density image. Biomech Model Mechanobiol .

Veenland JF, Grashuis JL & Gelsema ES (1998) Texture analysis in radiographs: the influence of modulation transfer function and noise on the discriminative ability of texture features. Med Phys 25(6): 922–936.

Viceconti M, Bellingeri L, Cristofolini L & Toni A (1998) A comparative study on different methods of automatic mesh generation of human femurs. Med Eng Phys 20(1): 1–10.

Vokes TJ, Giger ML, Chinander MR, Karrison TG, Favus MJ & Dixon LB (2006) Radiographic texture analysis of densitometer-generated calcaneus images differentiates postmenopausal women with and without fractures. Osteoporos Int 17(10): 1472–1482.

Vokes TJ, Pham A, Wilkie J, Kocherginsky M, Ma SL, Chinander M, Karrison T, Bris O & Giger ML (2008) Reproducibility and sources of variability in radiographic texture analysis of densitometric calcaneal images. J Clin Densitom 11(2): 211–220.

Voo L, Armand M & Kleinberger M (2004) Stress Fracture Risk Analysis of the Human Femur Based on Computational Biomechanics. Johns Hopkins apl technical digest 25(3): 223–230.

Wakao N, Harada A, Matsui Y, Takemura M, Shimokata H, Mizuno M, Ito M, Matsuyama Y & Ishiguro N (2009) The effect of impact direction on the fracture load of osteoporotic proximal femurs. Med Eng Phys 31(9): 1134–1139.

Wallace BA & Cumming RG (2000) Systematic review of randomized trials of the effect of exercise on bone mass in pre- and postmenopausal women. Calcif Tissue Int 67(1): 10–18.

Wang Q, Teo JW, Ghasem-Zadeh A & Seeman E (2009) Women and men with hip fractures have a longer femoral neck moment arm and greater impact load in a sideways fall. Osteoporos Int 20(7): 1151–1156.

Weerdesteyn V, Groen BE, van Swigchem R & Duysens J (2008) Martial arts fall techniques reduce hip impact forces in naive subjects after a brief period of training. J Electromyogr Kinesiol 18(2): 235–242.

Wei HW, Sun SS, Jao SH, Yeh CR & Cheng CK (2005) The influence of mechanical properties of subchondral plate, femoral head and neck on dynamic stress distribution of the articular cartilage. Med Eng Phys 27(4): 295–304.

White SC, Atchison KA, Gornbein JA, Nattiv A, Paganini-Hill A & Service SK (2006) Risk factors for fractures in older men and women: The Leisure World Cohort Study. Gend Med 3(2): 110–123.

WHO (1994) Assessment of fracture risk and its application to screening for postmenopausal osteoporosis. Report of a WHO Study Group. World Health Organ Tech Rep Ser 843: 1–129.

Willig R, Keinanen-Kiukaaniemi S & Jalovaara P (2001) Mortality and quality of life after trochanteric hip fracture. Public Health 115(5): 323–327.

Wirtz DC, Schiffers N, Pandorf T, Radermacher K, Weichert D & Forst R (2000) Critical evaluation of known bone material properties to realize anisotropic FE-simulation of the proximal femur. J Biomech 33(10): 1325–1330.

Wirtz DC, Pandorf T, Portheine F, Radermacher K, Schiffers N, Prescher A, Weichert D & Niethard FU (2003) Concept and development of an orthotropic FE model of the proximal femur. J Biomech 36(2): 289–293.

Wolff J (1892) Das Gesetz der transformation der Knochen. Translation by Maquet, P & Furlong, R: The law of bone remodelling. Berlin, 1986: Springer-Verlag .

Wolff I, van Croonenborg JJ, Kemper HC, Kostense PJ & Twisk JW (1999) The effect of exercise training programs on bone mass: a meta-analysis of published controlled trials in pre- and postmenopausal women. Osteoporos Int 9(1): 1–12.

Yang H, Ma X & Guo T (2010) Some factors that affect the comparison between isotropic and orthotropic inhomogeneous finite element material models of femur. Med Eng Phys 32(6): 553–560.

Yang L, Peel N, Clowes JA, McCloskey EV & Eastell R (2009) Use of DXA-based structural engineering models of the proximal femur to discriminate hip fracture. J Bone Miner Res 24(1): 33–42.

Youm T, Koval KJ, Kummer FJ & Zuckerman JD (1999a) Do all hip fractures result from a fall? Am J Orthop (Belle Mead NJ) 28(3): 190–194.

Youm T, Koval KJ & Zuckerman JD (1999b) The economic impact of geriatric hip fractures. Am J Orthop (Belle Mead NJ) 28(7): 423–428.

Zebaze RM, Jones A, Welsh F, Knackstedt M & Seeman E (2005) Femoral neck shape and the spatial distribution of its mineral mass varies with its size: Clinical and biomechanical implications. Bone 37(2): 243–252.

Zheng G, Gollmer S, Schumann S, Dong X, Feilkas T & Gonzalez Ballester MA (2009) A 2D/3D correspondence building method for reconstruction of a patient-specific 3D bone surface model using point distribution models and calibrated X-ray images. Med Image Anal 13(6): 883–899.

Zheng G & Schumann S (2009) 3D reconstruction of a patient-specific surface model of the proximal femur from calibrated x-ray radiographs: a validation study. Med Phys 36(4): 1155–1166.

Zheng G (2010) Statistical shape model-based reconstruction of a scaled, patient-specific surface model of the pelvis from a single standard AP x-ray radiograph. Med Phys 37(4): 1424–1439.

Original articles

I Thevenot J, Pulkkinen P, Kuhn V, Eckstein F & Jämsä T (2010) Structural asymmetry between the hips and its relation to experimental fracture type. Calcified Tissue International 87(3): 203–210.

II Thevenot J, Pulkkinen P, Koivumäki J, Kuhn V, Eckstein F & Jämsä T (2009) Discrimination of Cervical and Trochanteric Hip Fractures Using Radiography-Based Two-Dimensional Finite Element Models. Open Bone Journal 1: 16–22.

III Koivumäki J, Thevenot J, Pulkkinen P, Salmi J, Kuhn V, Lochmüller E-M, Link T, Eckstein F & Jämsä T (2010) Does femoral strain distribution coincide with the occurrence of cervical vs. trochanteric hip fractures? Medical & Biological Engineering & Computing 48(7): 711–717.

IV Thevenot J, Koivumäki J, Pulkkinen P, Kuhn V, Eckstein F & Jämsä T (2011) Estimation of experimental hip fracture load using 3D finite element models derived from plain radiographs. Manuscript.

Original publications are not included in the electronic version of the dissertation.

1112. Kaakinen, Mika (2011) Functional microdomains in the specialized membranes of skeletal myofibres

1113. Nissinen, Antti (2011) Humoral immune response to phosphatidylethanol

1114. Vuoti, Maire (2011) Pohjoissuomalaisten suurten ikäluokkien tulevaisuudenkuvat ikääntymisestään, hyvinvoinnistaan ja sosiaali- ja terveyspalveluistaan

1115. Hakalahti, Anna (2011) Human β_1-adrenergic receptor : biosynthesis, processing and the carboxyl-terminal polymorphism

1116. Peltonen, Jenni (2011) *TP53* as clinical marker in head and neck cancer

1117. Kariniemi, Juho (2011) Magnetic resonance imaging-guided percutaneous abdominal interventions

1118. Suorsa, Eija (2011) Assessment of heart rate variability as an indicator of cardiovascular autonomic dysregulation in subjects with chronic epilepsy

1119. Mikkola, Ilona (2011) Prevalence of metabolic syndrome and changes in body composition, physical fitness and cardiovascular risk factors during military service

1120. Venhola, Mika (2011) Vesicoureteral reflux in children

1121. Naillat, Florence (2011) Roles of *Wnt4/5a* in germ cell differentiation and gonad development & *ErbB4* in polarity of kidney epithelium

1122. Nurmenniemi, Sini (2011) Analysis of cancer cell invasion with novel *in vitro* methods based on human tissues

1123. Kangas-Kontio, Tiia (2011) Genetic background of HDL-cholesterol and atherosclerosis : Linkage and case-control studies in the Northern Finnish population

1124. Cederberg, Henna (2011) Relationship of physical activity, unacylated ghrelin and gene variation with changes in cardiovascular risk factors during military service

1125. Miller, Brian (2011) Paternal age, psychosis, and mortality : The Northern Finland 1966 Birth Cohort, Helsinki 1951–1960 schizophrenia cohort, and Finnish Nonaffective Psychosis Cohort

1126. Tolvanen, Mimmi (2011) Changes in adolescents' oral health-related knowledge, attitudes and behavior in response to extensive health promotion

1127. Pirilä-Parkkinen, Kirsi (2011) Childhood sleep-disordered breathing – dentofacial and pharyngeal characteristics

Book orders:
Granum: Virtual book store
http://granum.uta.fi/granum/

UNIVERSITY OF OULU P.O.B. 7500 FI-90014 UNIVERSITY OF OULU FINLAND

ACTA UNIVERSITATIS OULUENSIS

ISBN 978-951-42-9609-3 (Paperback)
ISBN 978-951-42-9610-9 (PDF)
ISSN 0355-3221 (Print)
ISSN 1796-2234 (Online)

UNIVERSITY of OULU
OULUN YLIOPISTO